

 Open access • Posted Content • DOI:10.1101/2021.10.01.462764

## **Non-conserved metabolic regulation by LKB1 distinguishes human and mouse lung adenocarcinoma — Source link**

Benjamin D. Stein, John Ferrarone, Eric E Gardner, Jae Won Chang ...+14 more authors

**Institutions:** Cornell University, University of Chicago, Salk Institute for Biological Studies, Beth Israel Deaconess Medical Center

**Published on:** 02 Oct 2021 - bioRxiv (Cold Spring Harbor Laboratory)

**Topics:** KRAS, Mutation, Kinase, Flux (metabolism) and Mutant

Related papers:

- [Crosstalk of LKB1-regulated and PTEN-regulated signals in liver morphogenesis and tumor development in mice](#)
- [Effect of Mutant p53 Proteins on Glycolysis and Mitochondrial Metabolism.](#)
- [Mutant TP53 Posttranslational Modifications: Challenges and Opportunities](#)
- [Polymorphism of p53 in cancer prognosis](#)
- [Reduced HRASG12V-Driven Tumorigenesis of Cell Lines Expressing KRASC118S](#)

Share this paper:    

View more about this paper here: <https://typeset.io/papers/non-conserved-metabolic-regulation-by-lkb1-distinguishes-k0nywoqo6h>

## 1 **Non-conserved metabolic regulation by LKB1 distinguishes human and mouse lung** 2 **adenocarcinoma**

3  
4 Benjamin D. Stein<sup>1,11\*</sup>, John R. Ferrarone<sup>1,11</sup>, Eric E. Gardner<sup>1</sup>, Jae Won Chang<sup>2,6</sup>, David Wu<sup>1</sup>, Qiuying  
5 Chen<sup>3</sup>, Pablo E. Hollstein<sup>4,7</sup>, Min Yuan<sup>5</sup>, Roger J. Liang<sup>1,8</sup>, John S. Coukos<sup>2</sup>, Miriam Sindelar<sup>3,9</sup>, Bryan  
6 Ngo<sup>1,10</sup>, Steven S. Gross<sup>3</sup>, Reuben J. Shaw<sup>4</sup>, John M. Asara<sup>5</sup>, Raymond E. Moellering<sup>2</sup>, Harold Varmus<sup>1\*</sup>,  
7 Lewis C. Cantley<sup>1\*</sup>

8  
9 <sup>1</sup>Sandra and Edward Meyer Cancer Center, Weill Cornell Medicine, New York, NY 10065, USA. <sup>2</sup>Department of  
10 Chemistry, University of Chicago, Chicago, IL 60637, USA. <sup>3</sup>Department of Pharmacology, Weill Cornell Medicine,  
11 New York, NY 10065, USA. <sup>4</sup>Molecular and Cell Biology Laboratory, The Salk Institute for Biological Studies, La Jolla,  
12 CA 92037, USA. <sup>5</sup>Mass Spectrometry Core, Beth Israel Deaconess Medical Center, Boston, MA 02215, USA.  
13 <sup>6</sup>Current address: Emory University, Atlanta, GA 30322, USA. <sup>7</sup>Current address: Amgen, Thousand Oaks, CA 07004,  
14 USA. <sup>8</sup>Current address: University of Texas – Southwestern, Dallas, TX 75390, USA. <sup>9</sup>Current address: Washington  
15 University in St. Louis, Saint Louis, MO 63130, USA. <sup>10</sup>Current address: Memorial Sloan Kettering Cancer Center,  
16 New York, NY 10021, USA. <sup>11</sup>These authors contributed equally; \*correspondence e-mail: bds2005@med.cornell.edu;  
17 varmus@med.cornell.edu; lcantley@med.cornell.edu

18  
19 ***KRAS* is the most frequently mutated oncogene in human lung adenocarcinomas (hLUAD) and**  
20 **activating mutations in *KRAS* frequently co-occur with loss-of-function mutations in the tumor**  
21 **suppressor genes, *TP53* or *STK11/LKB1*. However, mutation of all three genes is rarely observed in**  
22 **hLUAD, even though engineered mutations of all three genes produces a highly aggressive lung**  
23 **adenocarcinoma in mice (mLUAD). Here we provide an explanation of this difference between**  
24 **hLUAD and mLUAD by uncovering an evolutionary divergence in regulation of the glycolytic**  
25 **enzyme triosephosphate isomerase (TPI1). Using *KRAS/TP53* mutant hLUAD cell lines, we show**  
26 **that TPI1 enzymatic activity can be altered via phosphorylation at Ser21 by the Salt Inducible**  
27 **Kinases (SIKs) in an LKB1-dependent manner; this allows modulation of glycolytic flux between**  
28 **completion of glycolysis and production of glycerol lipids. This metabolic flexibility appears to be**  
29 **critical in rapidly growing cells with *KRAS* and *TP53* mutations, explaining why loss of LKB1 creates**  
30 **a metabolic liability in these tumors. In mice, the amino acid at position 21 of TPI1 is a Cys residue**  
31 **which can be oxidized to alter TPI1 activity, allowing regulation of glycolytic flux balance without a**  
32 **need for SIK kinases or LKB1. Our findings reveal an unexpected role for TPI1 in metabolic**  
33 **reprogramming and suggest that LKB1 and SIK family kinases are potential targets for treating**  
34 ***KRAS/TP53* mutant hLUAD. Our data also provide a cautionary example of the limits of genetically**  
35 **engineered murine models as tools to study human diseases such as cancers.**

36  
37 Lung cancer remains the most common cause of cancer mortality in the United States and worldwide, due  
38 to high incidence coupled with poor response to standard-of-care therapies in most patients.<sup>1</sup> Metabolic  
39 reprogramming is a cancer hallmark, required to support tumorigenesis in diverse environments.<sup>2,3</sup> Despite  
40 improvements in our understanding of metabolic discrepancies between normal and oncogenic tissues,  
41 accurately modeling and exploiting these differences for therapeutic intervention has achieved only marginal  
42 success.

43  
44 Inherent differences between humans and mice may have significant effects on tumor development  
45 through divergent mechanisms of response to the oxidative environment and to metabolic determinants.<sup>4</sup>  
46 The nature and extent of such differences are unknown, but their mechanisms may illuminate unidentified  
47 molecular targets for therapy. Therefore, we sought to identify differences between human and mouse lung  
48 adenocarcinomas (hLUAD and mLUAD) with the most common genotype, mutated *KRAS* and *TP53* (KP-  
49 mutant) and determine the effects of loss of the tumor suppressor, *LKB1*, on metabolic regulation and the  
50 growth of such tumors.

51  
52  
53

## 54 **Co-occurrence of *KRAS*, *TP53* and *LKB1* mutations differentially affects growth of human and** 55 **mouse LUADs**

56  
57 We used the TCGA PanCancer Atlas to determine the frequency of co-occurrence of mutations in the three  
58 most commonly mutated genes in hLUAD - *KRAS*, *TP53* and *LKB1* - and found that only 8 of 511 tumors  
59 carried mutations in all three genes (**Figure 1A**). A Fisher's Exact test showed that the co-occurrence of  
60 *LKB1* and *TP53* mutations in hLUADs with a *KRAS* mutation was less frequent than expected by chance,  
61 based on the overall frequency of mutations in these three genes, with an odds ratio of 0.35 and a P-value  
62 of 0.01 (**Figure 1B**). No similar reduction was observed in the co-mutation of *TP53* and *LKB1* in the  
63 absence of *KRAS* mutations (odds ratio = 0.95; p-value of 0.87) (**Figure 1B**). A second data set from  
64 Memorial Sloan Kettering Cancer Center consisting of 1,357 lung cancer patients revealed similar  
65 exclusivity of triple mutant cases (**Figure S1A and S1B**).<sup>5</sup>

66  
67 While mutations in *KRAS*, *TP53* and *LKB1* together are rare in hLUAD, previous studies have shown  
68 that genetically engineered mouse models (GEMMs) harboring conditional mutations in all three genes  
69 develop mLUAD that is more aggressive and more likely to metastasize than mLUAD with only two of these  
70 genes mutated.<sup>6-9</sup> To investigate this discrepancy between LUAD in human patients and mouse models, we  
71 first generated isogenic clones of human KP cell lines with and without *LKB1* deficiency and compared them  
72 to existing GEMM-derived mouse tumor lines with parallel genotypes.<sup>8</sup> The human KP lines engrafted and  
73 formed tumors *in vivo*, whereas isogenic lines in which *LKB1* was deleted (KPL) did not (**Figure 1C**).  
74 Furthermore, human KP lines readily formed spheroids in organotypic culture, but KPL lines did not (**Figure**  
75 **S1C**). In contrast, GEMM-derived KP and KPL lines both formed tumors *in vivo* and spheroids *in vitro*  
76 (**Figures 1D and S1D**).

77  
78 To determine whether these observations were attributable to *LKB1* kinase activity, wildtype or  
79 kinase-inactive (K78I) *LKB1* were re-expressed in isogenic KPL hLUAD lines derived from two human KP  
80 lines. We first verified that wildtype *LKB1* restored the activity of AMP-activated protein kinase (AMPK), a  
81 known substrate of *LKB1*, under conditions of energy stress. Glucose restriction caused *LKB1*-dependent  
82 phosphorylation of AMPK at Thr172 and of its downstream substrates (Acetyl CoA Carboxylase (ACC) at  
83 Ser79, Raptor at Ser792, and Unc-51 Like autophagy activating Kinase 1 (ULK1) at Ser555) (**Figure 1E**  
84 **and Figure S1E**). Expression of wildtype (WT), but not kinase-inactive (KI), *LKB1* rescued growth of the  
85 xenografts in immunodeficient mice, suggesting that *LKB1* kinase activity is required to support tumor  
86 formation by human KP LUAD cells (**Figure 1F**).

## 87 88 **Phosphorylation of human TPI1 is *LKB1*-dependent**

89  
90 Since *LKB1* phosphorylates and activates a family of AMPK-related Ser/Thr protein kinases (AMPKRs)  
91 involved in regulating various metabolic and stress response pathways, we used comprehensive  
92 quantitative phospho-proteomics under glucose-limited conditions to assess differences in protein  
93 phosphorylation between KP and KPL isogenic human lines. Phosphorylation of Ser21 on the glycolytic  
94 enzyme Triosephosphate Isomerase (TPI1) was one of the most significantly down-regulated  
95 phosphorylation events observed when comparing KPL to KP (**Figure 2A, S2A and S2B**). As expected, we  
96 also observed reduced phosphorylation of Ser108 in the beta subunits of AMPK: PRKAB1, and PRKAB2,  
97 each required for enzymatic activity (**Figures S2B**). In contrast, using the same experimental design with  
98 tumor-derived mouse cell lines, we did not detect phosphorylation of Tpi1 in cells with either KP or KPL  
99 genotypes (**Figure S2C**).

100  
101 To assess if restoration of *LKB1* kinase activity re-established phosphorylation of TPI1 during  
102 metabolic stress, we used quantitative proteomics and phospho-proteomics to analyze human KPL cells  
103 expressing WT or KI *LKB1* in parallel with KP and KPL cells under glucose-limited conditions. Ser21  
104 phosphorylation (p-Ser21) on TPI1 was again one of the most significantly reduced phosphorylation sites  
105 when KPL cells and KPL cells expressing KI *LKB1* were compared with KP cells and KPL cells expressing  
106 WT *LKB1* (**Figure 2B**). Furthermore, quantification of phosphopeptide ion intensities within individual

107 genotypes confirmed restoration of p-Ser21 levels in human KPL lines expressing WT, but not KI LKB1  
108 (**Figure S2D**), without significant variation in the abundance of TPI1 protein.

### 110 **Phosphorylation of TPI1 regulates triose phosphate levels**

111  
112 To examine the possibility that loss of regulation of TPI1 in hLUAD might explain selection against the KPL  
113 genotype, we studied the metabolic consequences of LKB1 deficiency. It is known that TPI1 controls the  
114 interconversion of the triose phosphates, dihydroxyacetone phosphate (DHAP) and glyceraldehyde-3-  
115 phosphate (GAP), both of which are generated from the upstream glycolytic intermediate fructose-1,6-  
116 bisphosphate (1,6-FBP) by aldolase. This conversion in carbon metabolism lies at a critical bifurcation  
117 point: one product, GAP, is used for glycolysis and energy homeostasis, whereas the other, DHAP, is used  
118 for lipid synthesis, cellular growth, and has recently been shown to activate the mammalian Target of  
119 Rapamycin protein kinase (mTOR).<sup>10</sup> Additionally, previous studies have shown that increased oxidative  
120 burden due to *KRAS* and/or *TP53* mutations cause metabolic flux to primarily flow through the oxidative  
121 Pentose Phosphate Pathway (oxPPP) to increase reductive potential and restore redox balance to  
122 overcome this liability.<sup>11-13</sup>

123  
124 We next assessed the influence of LKB1-dependent phosphorylation on TPI1 activity by measuring  
125 the pools of GAP and DHAP in KP and KPL hLUAD cell lines. Due to the inherent instability and complex  
126 chromatographic separation of the triose phosphates, we used *in situ* chemical-trapping metabolomics with  
127 hydroxylamine labeling of live cells under normal and glucose limited conditions prior to lysis to create  
128 stable adducts and measured them (**Figure 2C and S2E**).<sup>14</sup> These analyses confirmed relative elevation of  
129 DHAP in KPL lines, further suggesting that TPI1 phosphorylation limited DHAP accumulation to maintain  
130 GAP for glycolysis, crucial under glucose-limited conditions (**Figure 2D**). Additionally, a parallel analysis  
131 including KPL cell lines expressing WT and KI LKB1 with the same method revealed that levels of GAP and  
132 DHAP in WT LKB1 wildtype lines more accurately recapitulated endogenous levels in KP human cells, while  
133 DHAP remained elevated in the LKB1-KI cells (**Figure S2F**). Furthermore, steady-state analysis revealed  
134 that human KPL cells had a significant increase in glycerol-3-phosphate, the next metabolic intermediate in  
135 the lipid and triglyceride synthesis pathway under normal and low glucose conditions (**Figure 2E**).  
136 Collectively, the observed changes in metabolites and phosphorylation of human TPI1 suggested that LKB1  
137 regulates distribution of glycolytic metabolites via the triose phosphates through a regulatory  
138 phosphorylation site in TPI1.

### 140 **Non-conserved amino acid sequence of TPI1 requires LKB1 to regulate its multimeric state in 141 human but not mouse LUAD**

142  
143 To determine whether differences between LKB1 loss in human and mouse LUAD cells could be explained  
144 by differences in regulation of TPI1/Tpi1, we explored the evolutionary conservation of the primary amino  
145 acid sequence surrounding position 21 of this enzyme. Ser21 and the surrounding residues are conserved  
146 in most mammals and many other metazoan organisms, including yeast. However, in mouse and rat Tpi1,  
147 Ser21 has been replaced by a cysteine (**Figure 3A**). In a published crystal structure of human TPI1, the  
148 hydroxyl moiety of Ser21 is located at a region of subunit:subunit interactions, stabilizing the homodimer.  
149 Notably, the nearby residues Arg18 and Lys19 form inter-subunit electrostatic interactions predicted to  
150 further stabilize the highly active homodimeric state. This structure raises the possibility that  
151 phosphorylation of Ser21 could produce intra-subunit charge interactions with Arg18 and/or Lys19,  
152 interfering with the ability of these amino acids to confer stability to the dimer, thereby altering enzymatic  
153 activity (**Figure 3B**).<sup>15</sup> Since the sulfur atom of Cys21 in rodent Tpi1 could be oxidized to sulfinic or sulfonic  
154 acid, mimicking phosphorylation of Ser21, it is possible that rodents have a mechanistic alternative to  
155 phospho-dependent regulation of TPI1 activity. This could explain differences in the response to loss of  
156 LKB1 in mouse and human tumors, circumventing the requirement for LKB1 activity in murine tumors.

157  
158 Based on the structural features of human and mouse TPI1/Tpi1, we next asked whether the loss of  
159 LKB1 kinase activity, which prevents phosphorylation of human TPI1 at Ser21, would differentially affect the  
160 dimerization and activity of this enzyme in cells from the two species. We used native gel electrophoresis

(BN-PAGE) and western blotting to determine the proportions of monomeric and dimeric TPI1 in extracts of two human KP cell lines, in the presence and absence of LKB1, when cells are grown under normal glucose conditions (**Figure 3C**). Loss of LKB1 promoted the dimeric (more slowly migrating) form of the human protein; conversely, cell lines expressing LKB1 had increased monomeric (more rapidly migrating) TPI1 (Figure 3C). Thermal Proteome Profiling (TPP) was also used to measure the thermal stability of TPI1 proteoforms.<sup>16,17</sup> The  $\Delta T_m$  (measured at 0.5 fraction denatured) of the phosphorylated variant was 5.8°C lower than that of unmodified TPI1, further supporting the prediction that phosphorylation of Ser21 disrupts TPI1 dimerization (**Figure 3D**).

In contrast, we observed no changes in the ratio of the monomeric and dimeric forms of mouse Tpi1 in KP versus KPL mLUAD cell lines at high (11.1 mM) or low (0.5 mM) glucose concentrations (**Figure 3E**). However, acute treatment of the mouse lines with the oxidant peroxide caused a dramatic shift towards the rapidly migrating (monomeric) form of Tpi1 in low glucose medium, regardless of Lkb1 status (Figure 3E). Additionally, peroxide treatment caused a similar shift towards monomeric Tpi1 under high (11.1 mM) glucose conditions in KPL, but not KP mouse cells (Figure 3E), consistent with earlier reports that loss of Lkb1 increases basal oxidative stress.<sup>18-21</sup>

To further explore the functional significance of the amino acid difference at position 21 of TPI1 and Tpi1 and its effect on homodimer formation, we created an allelic panel of FLAG-HA-tagged TPI1 variants expressed as transgenes in human KP cells following deletion of endogenous TPI1. We observed that replacement of Serine with Alanine (S21A) increased recovery of both the transgenic and remaining endogenous TPI1 by immunoprecipitation, implying that an inability to phosphorylate position 21 of TPI1 stabilized the TPI1 dimer. In contrast, the phospho-mimetic S21D mutant form of TPI1 or a mutant in which Ser21 is replaced by an oxidizable cysteine (S21C) significantly reduced co-immunoprecipitation of the remaining endogenous TPI1 (**Figure 3F**). These findings were further confirmed when TPI1 variants from the allelic panel were analyzed by BN-PAGE. Wildtype transgenic human TPI1 was found in both the dimeric and monomeric states, but the S21A mutant was detected solely in the dimeric state, and the S21C variant was mostly monomeric (**Figure 3G**). Collectively, these findings support the conclusion that phosphorylation of human TPI1 or oxidation of murine Tpi1 destabilizes its dimeric form, providing a structural mechanism by which TPI1/Tpi1 activity can be regulated in response to LKB1-dependent phosphorylation or by oxidative stress.

### **LKB1-activated members of the Salt Inducible Kinase family phosphorylate human TPI1**

We next sought to determine whether human TPI1 is phosphorylated directly by LKB1 or by one of the downstream LKB1-dependent Ser/Thr protein kinases of the AMPKR family; these kinases are known to mediate responses to various metabolic stresses, all of which require phosphorylation by LKB1 for activity (**Figure 4A**).<sup>22-24</sup>

To determine whether AMPKR kinases are directly responsible for TPI1 phosphorylation downstream of LKB1, we monitored phosphorylation of Ser21 in TPI1 in a panel of human *KRAS*;*LKB1*-mutant cell lines in which sub-families of the AMPKR kinases have been genetically eliminated, after restoring stable expression of WT LKB1 from a transgene (**Figure 4B**).<sup>7</sup> Restoration of LKB1 increased the phosphorylation of Ser21 in TPI1, consistent with results in Figure 2B and S2D, and deletion of the Salt Inducible Kinase (SIK) subfamily significantly reduced Ser21 phosphorylation (**Figure 4B**). Deletion of other AMPKR super-family members [the Microtubule Affinity Regulating Kinases (MARKs), the NUA Family Kinases (NUAKs), the Brain-Specific Serine/Threonine-Protein Kinases (BRSKs), the catalytic subunits of AMPK, and SNF Related Kinase (SNRK)] did not have significant effects on Ser21 phosphorylation of TPI1. Furthermore, by analyzing specific combinations of deletions of SIK family members, we found that SIK1 and SIK3 together made the greatest contribution to phosphorylation of Ser21 in TPI1 (**Figure S3A**).

In agreement with the concept that the SIK sub-family of protein kinases drive phosphorylation of Ser21 in TPI1, phosphorylation of Ser551 in SIK3, known to regulate activity through altering molecular association, was one of the most significantly down-regulated phosphorylation sites in the LKB1-deleted,

215 KP-mutant hLUAD cell lines (Figure S2A).<sup>25,26</sup> Additionally, phosphorylation of the regulatory sites in a SIK-  
216 family substrate, CREB Regulated Transcription Coactivator 3 (CRTC3), was also down-regulated in KPL  
217 versus KP human lines (Figures S2A and S2B). Furthermore, we found that the amount of *SIK1* mRNA  
218 was significantly increased upon inactivation of *LKB1* in multiple human KP lines, suggesting that a  
219 signaling network might increase transcription of *SIK1* via a feedback mechanism to recover SIK activity  
220 after loss of *LKB1* (Figure S3B).

221  
222 We next asked if SIK family kinases were responsible for phosphorylation of TPI1 in human KP  
223 lines that express *LKB1* from the endogenous *LKB1* locus. We generated a series of cell lines deficient in  
224 members of the *SIK* gene family, including two *SIK1/2/3* triple knockout lines (SIK TKO). Analysis of this  
225 series of cell lines by western blot confirmed significant deletion of all SIK family members in the SIK TKO  
226 lines (Figure S3C). A quantitative proteomic analysis of differences between SIK WT and SIK TKO cells  
227 revealed that *KRAS* was among the most significantly down-regulated proteins (Figure 4C). This  
228 observation is consistent with SIK family enzymes being critical for cell growth when mutant *KRAS* is  
229 present and *TP53* is mutated. Measurement of the TPI1 p-Ser21 tryptic peptide from cells with various  
230 combinations of *SIK1*, *SIK2* and *SIK3* deletions argues that each of these kinases contribute to  
231 phosphorylation of TPI1 at Ser21 in human KP cells (Figure 4D).

232  
233 Taken together, these results indicate that in the KP hLUAD cell lines investigated, the SIK family of  
234 *LKB1*-regulated protein kinases appear to dominate the phosphorylation of Ser21 in TPI1, although deletion  
235 of all three SIK family members did not eliminate phosphorylation at this site, suggesting that other *LKB1*-  
236 regulated protein kinase may also contribute to TPI1 phosphorylation or compensate for loss of the SIK  
237 kinases. Our results suggest that an *LKB1* inhibitor might be an effective therapy for KP mutant hLUADs,  
238 though there are likely to be significant toxicities associated with the inhibition of *LKB1*. An alternative,  
239 potentially less toxic therapy would inhibit a sub-group of *LKB1*-regulated protein kinases, including the SIK  
240 family kinases, in *KRAS*; *TP53* human lung adenocarcinoma.

## 241 242 243 Discussion

244  
245 Although much progress has been made using GEMMs to decipher mechanisms of tumor initiation and  
246 progression, comparisons of human and mouse tumors often lead to conflicting observations.<sup>27</sup> In  
247 particular, accurately recapitulating the tumor metabolic environment remains a significant challenge, but an  
248 important one, since discrepancies between mouse and human tumors are likely to have implications in  
249 development of novel therapeutic agents.<sup>28</sup> Here we provide a mechanistic explanation for why the loss of  
250 *LKB1* in hLUADs driven by *KRAS* and *TP53* mutations is a rare event that appears to be selected against in  
251 human tumors, but not in mouse tumors, where the loss of *Lkb1* enhances tumorigenesis and metastasis.

252  
253 Several recent reports have implicated the SIK kinases as effectors of *LKB1*-mediated tumor  
254 suppression in *Kras*- and *Kras*; *Tp53*-mutant mLUAD; however similar findings have not been reported in  
255 hLUADs.<sup>7,29</sup> Here we find that this discrepancy may be due, at least in part, to a single amino acid  
256 difference between rodent and other metazoan versions of the glycolytic enzyme TPI1. In turn, that  
257 difference can influence subsequent metabolic events, that determine the flow of glucose-derived tri-carbon  
258 substrates into pathways for glycolysis or lipid synthesis. In humans, the abundance of the products of TPI1  
259 is governed by the *LKB1*-SIK-TPI1 signaling axis that we have elucidated in this manuscript. In rodents, the  
260 substitution of an oxidizable cysteine for a phosphorylatable serine at residue 21 of *Tpi1* enables direct  
261 redox regulation, circumventing the requirement for regulation by *LKB1*-SIK-mediated phosphorylation. Our  
262 biochemical, proteomic, and metabolomic data support the conclusion that phosphorylation of TPI1 in  
263 hLUAD regulates the biophysical distribution of monomeric and dimeric forms, altering enzymatic activity  
264 and in turn triose phosphate pools. This reduces the conversion of GAP to DHAP, an energetically downhill  
265 reaction, and thereby shifts the balance away from glycerol lipid production and towards alternate metabolic  
266 pathways, including glycolysis and the TCA cycle. Regulation of metabolites at this central point in the  
267 glycolytic pathway could help to overcome metabolic stresses experienced during tumorigenesis and to  
268 improve the efficiency of energy production. In addition, this regulation allows rapidly growing cells to

269 balance pathways for lipid synthesis versus serine/glycine synthesis. Collectively, these metabolic  
270 differences could strongly influence a wide range of pro-tumorigenic processes and have significant effects  
271 on tumor cell phenotype, all of which warrant future study. Additional features of these phenomena - such  
272 as how specific *KRAS* and *TP53* mutations influence this phenotype and their contributions to the response  
273 to metabolic and oxidative stresses - have yet to be deciphered.

274  
275 Knowledge of the differences in human and mouse TPI1/Tpi1 may not only explain the different  
276 consequences of loss of LKB1 in human and mouse LUADs but may also help to design next-generation  
277 mouse models in which the mechanisms of metabolic regulation of human cancers are more accurately  
278 replicated. Furthermore, the research reported here suggests that selective inhibitors of LKB1 or of SIK  
279 family protein kinases could be effective in treating human *Kras*/*TP53* mutant lung cancers or other cancers  
280 with *KRAS*/*TP53* mutations. But our work also raises the cautionary note that preclinical trials with such  
281 inhibitors would likely fail in currently available GEMMs with *Kras* and *Tp53* mutations.

282  
283 Finally, the observations reported here also reveal new ways for LKB1 to regulate metabolism,  
284 beyond its known capacity to respond to cellular energy levels through activation of AMPK.<sup>30</sup> While  
285 enzymes such as hexokinase, pyruvate kinase and phosphofructokinase have been intensely studied in  
286 regard to phosphorylation-dependent regulation in cancers, TPI1 has not been considered a likely site for  
287 cancer-dependent regulation of metabolic flux. Additional research is needed to understand how critical this  
288 regulation is to other types of human cancers and whether this knowledge can lead to new cancer therapies  
289 across multiple organ types and multiple mutational backgrounds.

## 291 **Data Availability**

292 All derived MS/MS data will be deposited on MASSive and ProteomeXchange.

## 294 **Supplemental Information**

295 Supplemental Information includes 3 supplemental figures.

## 297 **Acknowledgements**

298 We thank Kwok-Kin Wong for kindly providing GEMM derived LUAD cell-lines; 634T and *Lkb1*-t2. This  
299 work was supported, in part, by NIH grants; P01CA120964 (to L.C.C., R.J.S. and J.M.A.), R35CA197588 (to  
300 L.C.C.), R35-CA220538 (to R.J.S.), R01-DK080425 (to R.J.S.), R01AR076029 (to Q.C.) and R21ES032347  
301 (to Q.C.); NSF-CAREER CHE-1945442 (to R.E.M.) and the Alfred P. Sloan Foundation FG-2020-12839 (to  
302 R.E.M.). H.E.V. is the Lewis Thomas University Professor at Cornell University. J.R.F. is the Lee  
303 Cooperman Physician-Scientist of the Damon Runyon Cancer Research Foundation (DRG 18-18). E.E.G.  
304 is the Kenneth G. and Elaine A. Langone Fellow of the Damon Runyon Cancer Research Foundation  
305 (DRG-2343-18). B.N. is supported by a National Cancer Institute (NCI) of the National Institutes of Health  
306 (NIH) F99/K00 Career Transition Fellowship (F99CA234950).

## 308 **Author Contributions**

309 B.D.S., H.E.V., and L.C.C. conceived of and designed the study. B.D.S. guided and performed most  
310 experiments, performed all proteomics and biochemical experiments, metabolomics experiments and all  
311 computational analyses. J.R.F. performed experiments and analyzed clinical data. E.E.G., D.W. and B.N.  
312 assisted in xenograft studies in Figures 1C, 1D and 1F. E.E.G. performed 3D Matrigel experiments in  
313 Figure S1C. J.W.C., J.S.C. and R.E.M. performed and analyzed chemical trapping metabolomics data in  
314 Figure 2D. M.Y. and J.M.A. performed metabolomics analyses in Figures 2E. Q.C., M.S. and S.S.G.  
315 analyzed metabolomics experiments. P.E.H. and R.J.S. provided cell-lines and lysates utilized for  
316 proteomics in Figure 4B and S4A. R.J.L. performed experiments. B.D.S. wrote the manuscript, which was  
317 reviewed by all authors. H.E.V. and L.C.C. supervised the study.

322 **Competing Interests**

323 L.C.C. is a co-founder and member of the SAB and holds equity in Faeth Therapeutics, Volastra  
324 Therapeutics and Larkspur Therapeutics. He is also a co-founder, former member of the SAB and BOD  
325 and holds equity in Agios Pharmaceuticals. H.E.V. is a member of the SABs of Volastra, Dragonfly  
326 Therapeutics, and Surrozen. These companies are developing novel therapies for cancer. L.C.C.'s  
327 laboratory has previously received some financial support from Petra Pharmaceuticals. None of these  
328 companies are developing drugs related to the research in this paper. All other authors declare no  
329 competing interests.

330  
331  
332  
333  
334  
335  
336  
337  
338  
339  
340  
341  
342  
343  
344  
345  
346  
347  
348  
349  
350  
351  
352  
353  
354  
355  
356  
357  
358  
359  
360  
361  
362  
363  
364  
365  
366  
367  
368  
369  
370  
371  
372  
373  
374  
375



## 376 Figure Legends

377

### 378 **Figure 1. Co-occurrence of *KRAS*, *TP53* and *LKB1* mutations differentially affects growth of human** 379 **and mouse LUADs.**

380 (A) The Cancer Genome Atlas PanCancer Atlas oncoprint of co-occurrence of *KRAS*, *TP53* and *LKB1* in  
381 human lung adenocarcinoma patients. (B) Fisher's exact test of statistical likelihood of co-occurrence of  
382 *LKB1* and *TP53* mutations in a *KRAS* mutant or wildtype background respectively. (C) Graph of mean (+/-  
383 s.e.m.) tumor volumes of sub-cutaneous flank injections of H358 (*KRAS*; *TP53*) isogenic clones expressing  
384 Cas9 and a non-targeting (sgNT1.4 and sgNT1.6) or *LKB1*-specific (sgLKB1-2.1 and sgLKB13.2) guide  
385 RNA.  $1 \times 10^6$  cells implanted in right hind flank ( $n = 10$  per cohort). (D) Mean (-/+ s.e.m.) volumes of  
386 mouse 634T (KP) and *Lkb1*-t2 (KPL) lung adenocarcinoma allograft tumors.  $1 \times 10^4$  cells implanted in right  
387 hind flank ( $n = 10$  per cohort). (E) Western blot analysis of H358 (*KRAS*; *TP53*) isogenic clones (KP:  
388 sgNT1.4 and sgNT1.6; KPL: sgLKB1-2.1 and sgLKB1-3.2) and KPL lines with additional transgenic  
389 expression of guide RNA resistant *LKB1* wildtype (WT) (sgLKB1-2.1 + *LKB1* WT and sgLKB1-3.2 + *LKB1*  
390 WT) or *LKB1* kinase inactive (KI) (sgLKB1-2.1 + *LKB1* KI and sgLKB1-3.2 *LKB1* KI) and treated with 11.1  
391 mM or 0.5 mM glucose for 6 hours as indicated. Restoration of AMPK signaling in *LKB1* WT lines in  
392 response to 0.5 mM glucose validated by blotting for P-AMPK Thr172 and downstream substrates (P-ACC  
393 S79, P-ULK1 S555, P-Raptor S792). Similar results observed in three independent experiments and in an  
394 additional *KRAS*; *TP53* cell line, H2009 (Figure S1E). (F) Graph of mean (-/+ s.e.m.) tumor volumes of sub-  
395 cutaneous flank injections of H358 (*KRAS*; *TP53*) isogenic clones with transgenic expression of an empty  
396 vector (KO) or guide RNA resistant *LKB1* wildtype (*LKB1* WT) or *LKB1* kinase inactive (*LKB1* KI).  $1 \times 10^6$   
397 cells implanted in right hind flank ( $n = 10$  per cohort).

398

### 399 **Figure 2. Phosphorylation of human TPI1 is *LKB1*-dependent and regulates triose phosphate levels.**

400 (A) Volcano plot of quantitative phospho-proteomic data of genetic sensitivity in H2009 clones (2 KP clones  
401 and 2 KPL clones), two biological replicates each,  $N = 4$  per genotype. Cells grown in 0.5 mM glucose for 6  
402 hours. Phospho-peptides that pass statistical criteria ( $p$ -value  $< 0.05$ ) are highlighted in black, red and blue,  
403 peptides that do not satisfy this are colored grey. Phospho-peptides colored red satisfy a fold change  $> 1.5$ ;  
404 colored blue, fold change  $< -1.5$ . TPI1 P-Ser21 peptide labeled in purple text. (B) Volcano plot of  
405 quantitative phospho-proteomic data of genetic sensitivity in H2009 isogenic clones including clones with  
406 transgenic expression of guide RNA resistant wildtype (WT) or kinase inactive (KI) *LKB1* in *LKB1*-specific  
407 knockouts (sgLKB1-3.1 and sgLKB1-3.7) from Figure S1E, 4 biological replicates each. *LKB1* Loss-of-  
408 function (LOF) group consisted of merging *LKB1* knockout lines (KPL: sgLKB1-3.1 and sgLKB1-3.7) with  
409 lines expressing guide RNA resistant *LKB1* KI (KPL + *LKB1* KI: sgLKB1-3.1 + *LKB1* KI and sgLKB1-3.7 +  
410 *LKB1* KI); and compared to H2009 lines containing non-targeting guide RNA (KP: sgNT1.1 and sgNT1.2)  
411 merged with *LKB1* knockout lines expressing guide RNA resistant *LKB1* WT (KPL + *LKB1* WT: sgLKB1-3.1  
412 + *LKB1* WT and sgLKB1-3.7 + *LKB1* WT) at the phospho-peptide level. Cells were grown in 0.5mM  
413 glucose for 6 hours. Statistical criteria and color scheme same as for panel A. TPI1 P-Ser21 peptide  
414 labeled in purple text. (C) Schematic showing metabolites (shaded in the orange box) chemically labeled to  
415 create stable adducts. (D) *In-situ* chemical trapping metabolomics of hydroxylamine-labeled GAP and  
416 DHAP in H2009 clones (KP: sgNT1.1 and sgNT1.2; KPL: sgLKB1-3.1 and sgLKB1-3.7) treated in culture for  
417 6 hours with 11.1 mM or 0.5 mM respectively. Data presented are representative of three independent  
418 biological experiments each containing three technical replicates and reported as the mean (-/+s.e.m.). Cell  
419 number normalized across models 12 hours prior to assay and samples normalized to an exogenous  
420 standard,  $d_3$ -serine. Statistical significance determined by two-tailed paired t-test. (E) Normalized ion  
421 intensity of glycerol-3-phosphate from steady-state analysis of H2009 clones treated for 30 minutes with  
422 11.1 or 0.5 mM glucose. Analysis conducted in H2009 isogenic clones (KP: sgNT1.1 and sgNT1.2; KPL:  
423 sgLKB1-3.1 and sgLKB1-3.7) in biological triplicate and reported as the mean (-/+s.e.m.). Statistical  
424 significance determined by two-tailed paired t-test.

425

### 426 **Figure 3. *LKB1* regulates the multimeric state of TPI1 in KP-mutant hLUAD but not in mLUAD cell** 427 **lines due to an amino acid difference at position 21.**

428 (A) Sequence alignment of TPI1 amino acid residues 16 to 26 across species, showing conservation of  
429 Ser21 from *H. sapiens* to *S. Cerevisiae*, with cysteine at position 21 in mouse and rat Tpi1. Cartoon

430 comparing predicted side-chain chemistry, with oxidized cysteine and phosphorylated serine, is drawn  
431 below. **(B)** Crystal structure of TPI1 homodimer (cyan and green respectively) with critical residues  
432 highlighted in space-filling atoms. Serine 21 on the cyan monomer is highlighted in yellow. **(C)** Western  
433 blot analysis of Blue Native PAGE of human isogenic clones derived from H358 and H441 cell lines. Cells  
434 were grown under normal conditions (11.1 mM glucose). **(D)** Melting curve plot from Thermal Proteome  
435 Profiling of unmodified and Serine 21 phosphorylated TPI1. Analysis conducted in H2009 isogenic clones  
436 expressing Cas9 and a non-targeting (sgNT1.1 and sgNT1.2) or LKB1-specific (sgLKB1-3.1 and  
437 sgLKB13.7) guide RNA. **(E)** Western blot (Blue Native PAGE) of extracts from mLUAD cell lines. Cells  
438 were cultured in either 11.1 mM or 0.5 mM glucose for 6 hours then treated with 1 mM H<sub>2</sub>O<sub>2</sub> for 15 minutes.  
439 **(F)** Western blot of proteins co-immunoprecipitated from extracts of H358 cells expressing Cas9 and a non-  
440 targeting (FH-GFP cell line) or TPI1-specific (all other cell lines) guide RNA and transgenic expression of  
441 Flag-HA tagged GFP or guide RNA resistant TPI1 allelic variants using a polyclonal antibody against full-  
442 length TPI1. Cells were cultured in 11.1 mM glucose and treated with 250 μM Diamide or vehicle for 15  
443 minutes prior to collection. **(G)** Western blot (Blue Native PAGE) of extracts of H358 cell lines used for co-  
444 immunoprecipitation in panel F. Cells were cultured in 11.1 mM glucose.  
445

446 **Figure 4. Salt Inducible Kinases phosphorylate human TPI1 in KP hLUAD cell lines.**

447 **(A)** Cartoon depicting regulation of the AMPK-related (AMPKR) kinase family members by LKB1 and their  
448 downstream substrates. **(B)** Bar graph of normalized ion abundance for the TPI1-derived ser-21 phospho-  
449 peptide from extracts of A549 cell-lines infected with an empty vector or a vector expressing wild type LKB1;  
450 the indicated guide RNAs were used to inactivate members of the AMPKR subfamilies. Cell lines were  
451 cultured in 11.1 mM glucose prior to analysis. Ion intensities were normalized to identified non-  
452 phosphorylated variants across conditions to control for protein expression and reported as the mean (-/+  
453 s.e.m.). **(C)** Volcano plot of quantitative proteomic data used to compare protein expression in clones of  
454 H358 (2 KP clones and 2 KP SIK TKO clones, with 2 biological replicates of each). Cells were cultured in  
455 11.1 mM glucose for 6 hours before lysis. Proteins that pass statistical criteria (p-value <0.05) are  
456 highlighted in black, red and blue; those that do not satisfy this criterion are colored grey. Proteins  
457 highlighted in red satisfy the fold change threshold (>1.5) after triple deletion of SIK1,2,3. Proteins  
458 highlighted in blue satisfy the fold change threshold of < -1.5) for a decrease after SIK1,2,3 triple deletion.  
459 KRAS is labeled in purple text. **(D)** Bar graph of normalized ion abundance for the TPI1-derived, ser-21  
460 phospho-peptide in extracts of isogenic H358 cell-lines containing a non-targeting control (sgNT1.3) or SIK1  
461 specific (sgSIK1.3) guide RNA and additional control (NT1) SIK1 (sgSIK1) or dual SIK2 and SIK3  
462 (sgSIK2/3) guide RNAs. Ion intensities were normalized against identified non-phosphorylated variant  
463 across conditions. Cell lines were cultured in 11.1 mM glucose prior to lysis, analyzed in biological  
464 triplicate, and reported as the mean (-/+ s.e.m.).  
465  
466  
467  
468  
469  
470  
471  
472  
473  
474  
475  
476  
477  
478  
479  
480  
481  
482

TCGA - PanCancer Atlas



**B**

**KRAS Mutant**

		TP53	
		WT	Mut
LKB1	WT	69	49
	Mut	32	8

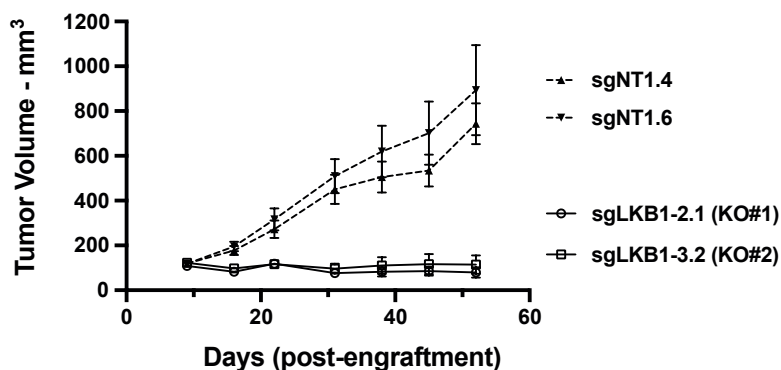
Odds Ratio: 0.35  
P-value: 0.01

**KRAS WT**

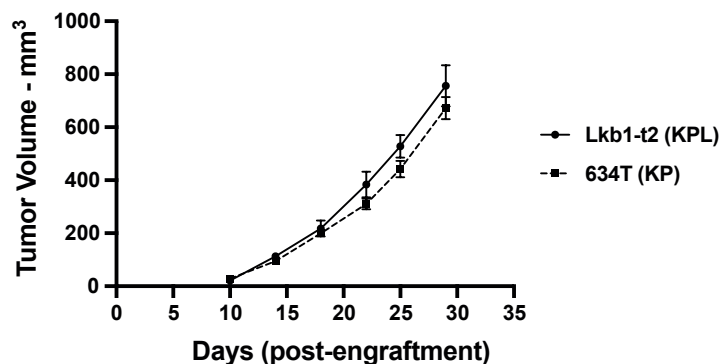
		TP53	
		WT	Mut
LKB1	WT	129	184
	Mut	17	23

Odds Ratio: 0.95  
P-value: 0.87

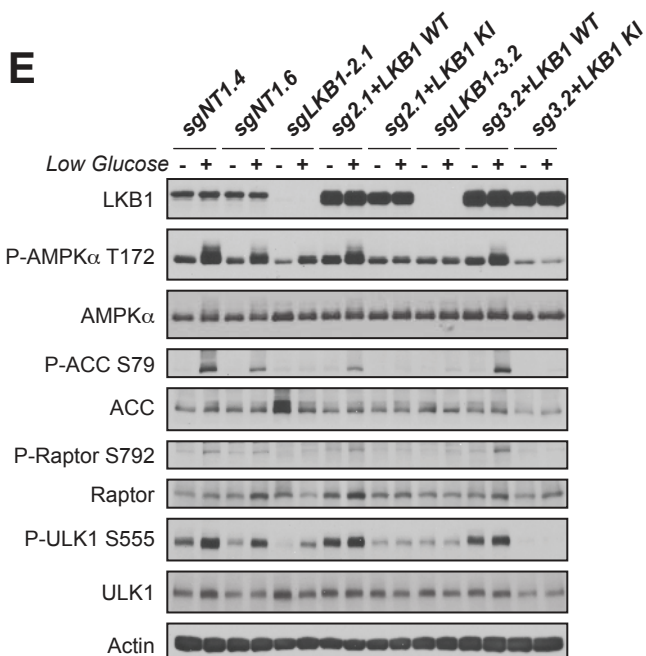
**C**



**D**



**E**



**F**

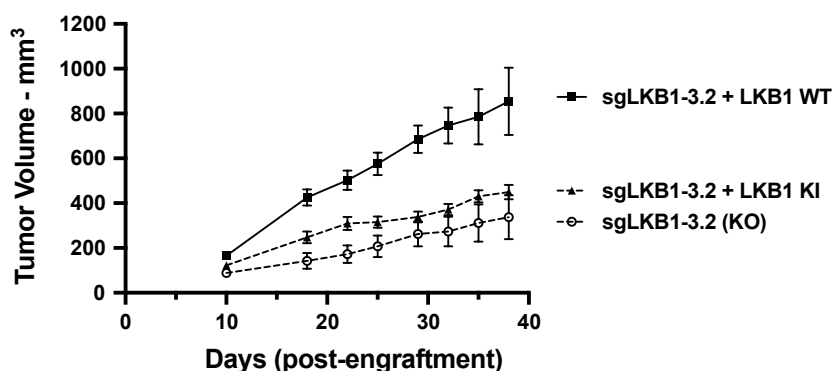


Figure 1

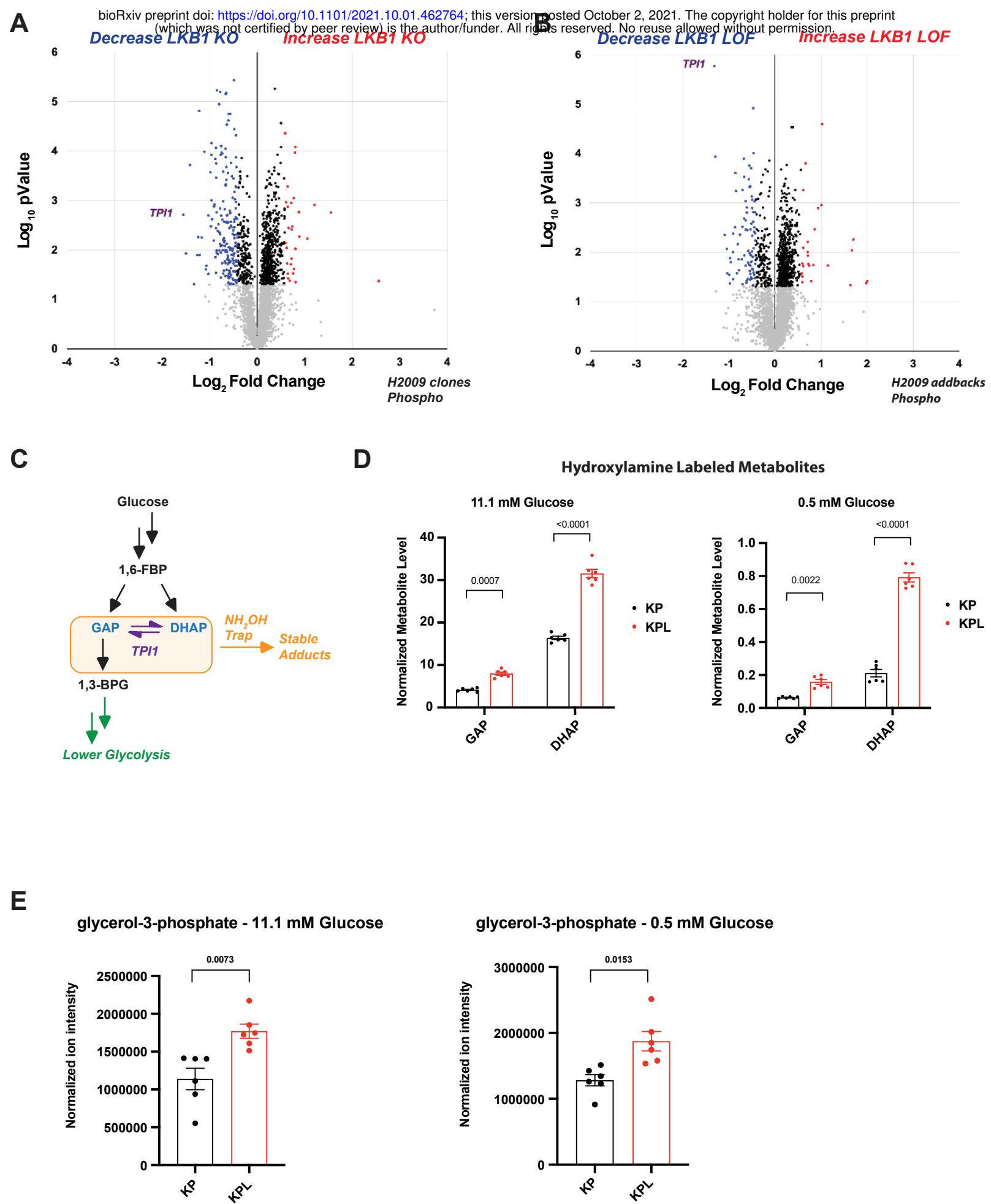
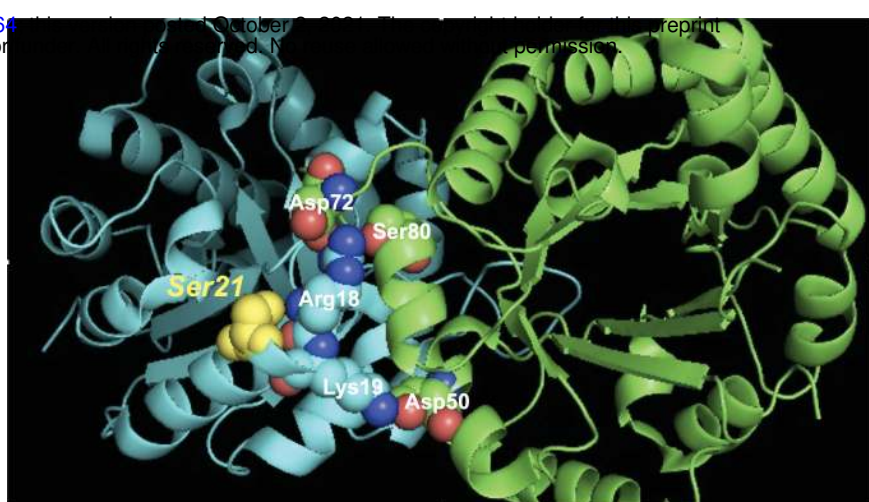
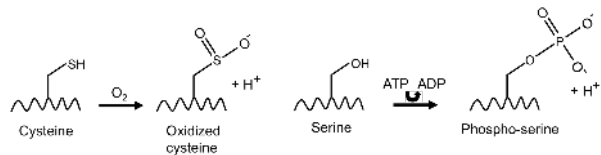


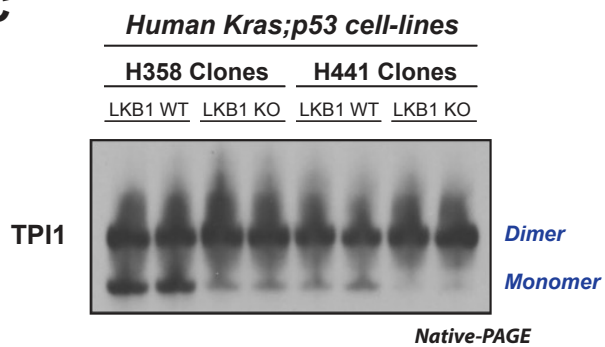
Figure 2

**A**

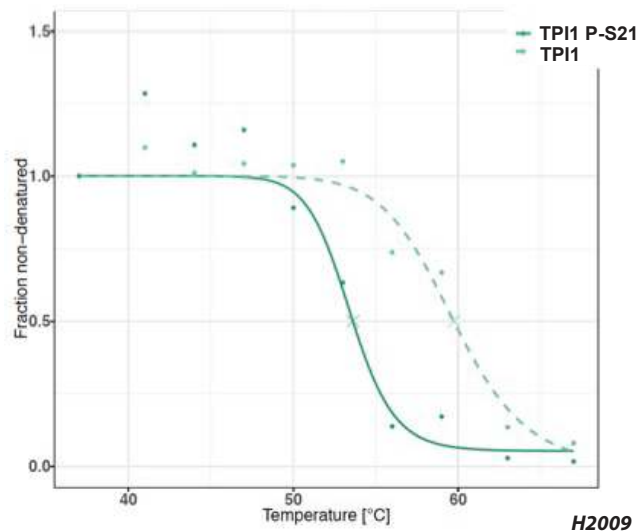
NG	R	Q	S	L	G	E	L	I	<i>Homo Sapiens</i>	
NG	R	K	Q	S	L	G	E	L	I	<i>Gorilla gorilla gorilla</i>
NG	R	K	Q	S	L	G	E	L	I	<i>Pan troglodytes</i>
NG	R	K	K	S	L	G	E	L	I	<i>Mus musculus</i>
NG	R	K	K	S	L	G	E	L	I	<i>Rattus norvegicus</i>
NG	D	K	K	S	L	T	E	L	I	<i>Xenopus tropicalis</i>
NG	D	K	E	S	L	G	E	L	I	<i>Danio rerio</i>
NG	D	Q	K	S	I	A	E	I	A	<i>Drosophila melanogaster</i>
NG	D	Y	A	S	V	D	G	I	V	<i>Caenorhabditis elegans</i>
NG	S	K	Q	S	I	K	E	L	V	<i>Saccharomyces cerevisiae</i>



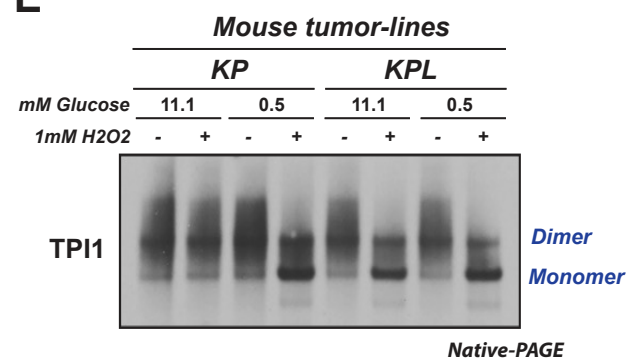
**C**



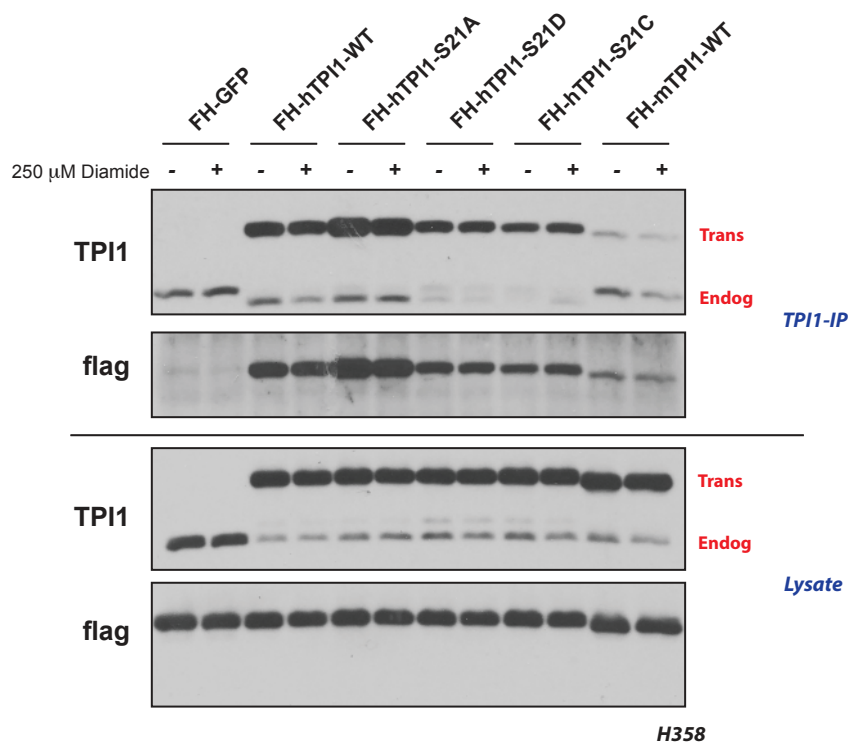
**D**



**E**



**F**



**G**

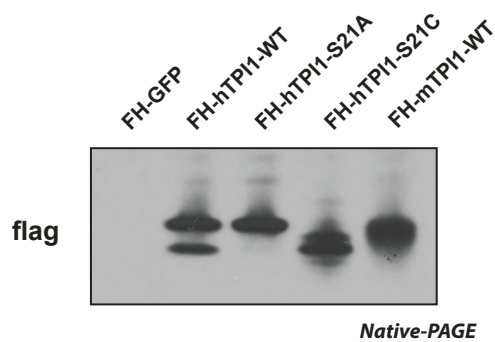
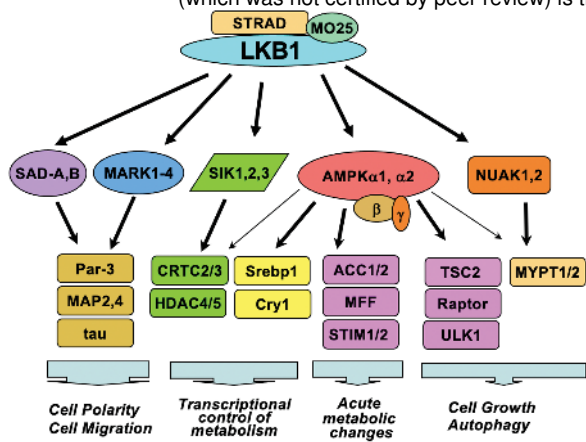
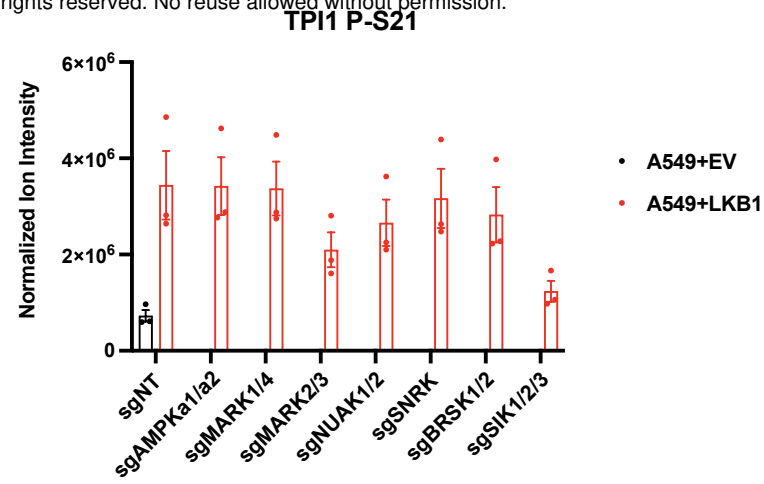


**Figure 3**

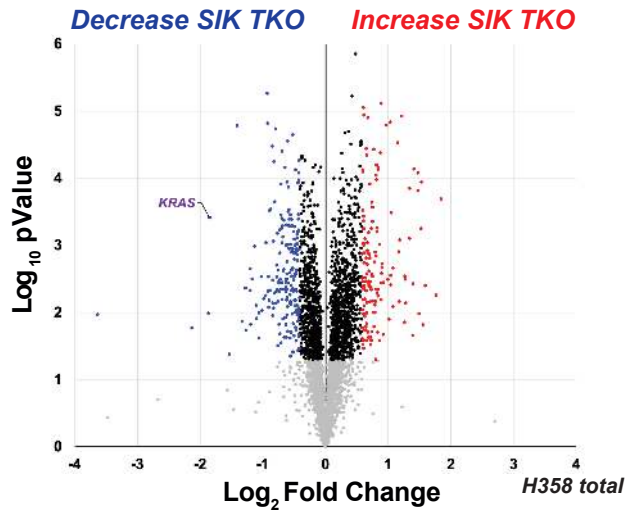
**A**



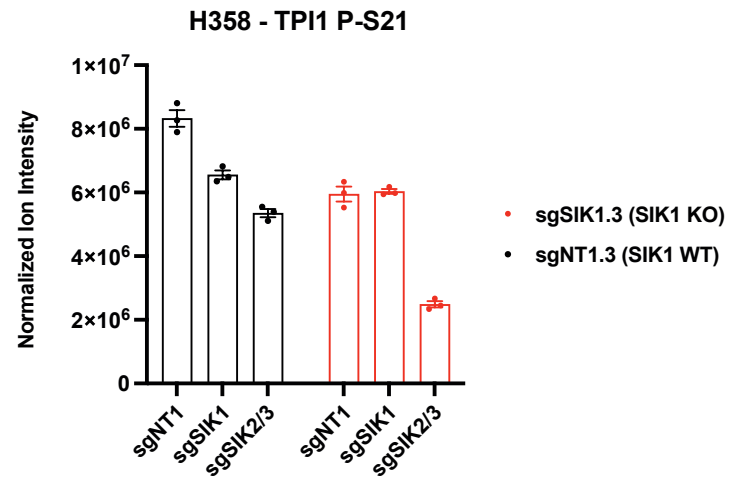
**B**



**C**



**D**



## 483 Supplemental Figure Legends

484

### 485 **Figure S1. Differential co-occurrence and effects of *KRAS*, *TP53* and *LKB1* mutations on human and** 486 **mouse LUADs**

487 **(A)** MSK Impact oncoprint of co-occurrence of *KRAS*, *TP53* and *LKB1* mutations in human lung  
488 adenocarcinomas, with Fisher's exact test of statistical likelihood of co-occurrence of *LKB1* and *TP53*  
489 mutations in a LUAD with a *KRAS* mutant or wildtype background. **(C)** 3D spheroid growth in Matrigel of  
490 isogenic clones of the H358 cell line labeled with a tdTomato fluorescent reporter and expressing CAS9 and  
491 non-targeting controls (sgNT1.4 and sgNT1.6) or *LKB1*-specific (sgLKB1-2.1 and sgLKB1-3.2) guide RNAs.  
492 5,000 cells were seeded into Matrigel and grown for 10 days in media changed every 24 hours. Images  
493 taken on EVOS fluorescence microscope under 4x magnification and filter to resolve tdTomato signal  
494 intensity and brightfield. **(D)** 3D spheroid growth in Matrigel of GEMM-derived mLUAD cell lines containing  
495 transgenic lentiviral expression of GFP under control of a CMV promoter. 5,000 cells were seeded into  
496 Matrigel and assay was conducted for 10 days in culture media changed every 24 hours. Images taken on  
497 EVOS fluorescence microscope under 10x magnification and filter to resolve GFP signal intensity and  
498 brightfield. **(E)** Western blot analysis of H2009 (*KRAS*; *TP53*) isogenic clones (KP: sgNT1.1 and sgNT1.2;  
499 KPL: sgLKB1-3.1 and sgLKB1-3.7) and lines with additional transgenic expression of guide RNA resistant  
500 *LKB1* wildtype (WT) (sgLKB1-3.1 + *LKB1* WT and sgLKB1-3.7 + *LKB1* WT) or *LKB1* kinase inactive (KI)  
501 (sgLKB1-3.1 + *LKB1* KI and sgLKB1-3.7 *LKB1* KI) and treated with 11.1 mM or 0.5 mM glucose for 6 hours  
502 as indicated. Restoration of AMPK signaling in *LKB1* WT lines in response to 0.5 mM glucose validated by  
503 blotting for P-AMPK Thr172 and downstream substrates (P-ACC S79, P-ULK1 S555, P-Raptor S792).  
504 Similar results observed in three independent experiments.

505

### 506 **Figure S2. Phosphorylation of human TPI1 is *LKB1*-dependent and regulates triose phosphate** 507 **levels.**

508 **(A and B)** Volcano plots for comparison of phospho-peptides enriched from lysates of H358 and H441  
509 isogenic clones respectively with and without *LKB1* [2 KP clones (H358: sgNT1.4 and sgNT1.6; H441:  
510 sgNT1.2 and sgNT1.4) and 2 KPL clones (H358: sgLKB1-2.1 and sgLKB1-3.2. H441: sgLKB1-2.2 and  
511 sgLKB1-3.3) with 2 biological replicates for each cell line]. Cells were grown in 0.5 mM glucose for 6 hours  
512 before lysis. Phospho-peptides that pass statistical criteria ( $p$ -value  $< 0.05$ ) are highlighted in black, red and  
513 blue, peptides that do not satisfy this criterion are colored grey. Phospho-peptides highlighted in red satisfy  
514 a fold-change threshold ( $> 1.5$ ) upon *LKB1* deletion; those highlighted in blue satisfy the fold change  
515 threshold ( $< -1.5$ ) upon *LKB1* deletion. Phospho-peptides referenced in the text (SIK3, CRT3, PRKAB1  
516 and PRKAB2) are labeled in purple text. **(C)** Volcano plot for comparison of quantitative phospho-proteomic  
517 data of genetic sensitivity in mLUAD cell-lines, 634T (KP) and *Lkb1-t2* (KPL) in biological triplicate for each  
518 condition. Analysis conducted on cells treated with 0.5mM glucose for 6 hours in culture. Statistical criteria  
519 and color scheme same as for panel A and B. **(D)** Average ion intensity of the H2009 (*KRAS*; *TP53*)  
520 isogenic clones (KP: sgNT1.1 and sgNT1.2; KPL: sgLKB1-3.1 and sgLKB1-3.7) and lines with additional  
521 transgenic expression of guide RNA resistant *LKB1* wildtype (WT) (sgLKB1-3.1 + *LKB1* WT and sgLKB1-  
522 3.7 + *LKB1* WT) or *LKB1* kinase inactive (KI) (sgLKB1-3.1 + *LKB1* KI and sgLKB1-3.7 *LKB1* KI) for the  
523 phospho-peptide containing Serine 21 of TPI1 from the experiments from which the volcano plot in Figure  
524 2B was derived. Bar graph depicts each genotype individually and shows restoration of TPI1  
525 phosphorylation in KPL lines expressing transgenic WT *LKB1* but not KI *LKB1*. Ion intensities were  
526 normalized to identified non-phosphorylated variant across conditions to control for protein expression; the  
527 relevant phospho-peptide was observed 3 times in each biological replicate. **(E)** Schematic showing  
528 hydroxylamine chemical labeling and conversion of the triose phosphates; GAP and DHAP to their oxime  
529 derivatives. **(F)** *In-situ* chemical trapping metabolomics of hydroxylamine-labeled GAP and DHAP in H2009  
530 clones (KP: sgNT1.1 and sgNT1.2; KPL: sgLKB1-3.1 and sgLKB1-3.7) and additionally lines with transgenic  
531 expression of guide RNA resistant *LKB1* wildtype (WT) (sgLKB1-3.1 + *LKB1* WT and sgLKB1-3.7 + *LKB1*  
532 WT) or *LKB1* kinase inactive (KI) (sgLKB1-3.1 + *LKB1* KI and sgLKB1-3.7 *LKB1* KI) and treated in culture  
533 for 6 hours with 11.1 mM or 0.5 mM respectively. Data presented are representative of three independent  
534 biological experiments each containing two technical replicates and reported as the mean ratio (GAP-  
535 trap/DHAP-trap) (-/+s.e.m.). Cell number normalized across models 12 hours prior to assay and samples  
536 normalized to an exogenous standard,  $d_3$ -serine.

537 **Figure S3. Members of the salt Inducible kinase family phosphorylate TPI1.**

538 **(A)** Bar graph of normalized ion abundance for the TPI1-derived Ser-21 phospho-peptide in extracts of  
539 A549 cell-lines expressing an empty vector or wild type LKB1 and guide RNAs specifically targeting  
540 combinations of members of the Salt Inducible Kinase family. Cell lines were cultured in 11.1 mM glucose.  
541 **(B)** Graphs depicting the mean mRNA level (+ s.d.) of the Salt Inducible Kinases in the indicated isogenic  
542 clones of H2009 (left) and H358 (right). **(C)** Western blots showing abundance of SIK1, SIK2 and SIK3 in  
543 H358 isogenic clones after exposure to the indicated guide RNAs for members of the SIK family. H358  
544 isogenic clones expressing Cas9 and containing non-targeting control (sgNT1.3 and sgNT1.4) or SIK1  
545 specific (sgSIK1.3 and sgSIK1.4) guide RNA and additional non-targeting (NT1), SIK1 (sgSIK1) or dual  
546 SIK2 and SIK3 (sgSIK2/3) guide RNAs.

547  
548  
549  
550  
551  
552  
553  
554  
555  
556  
557  
558  
559  
560  
561  
562  
563  
564  
565  
566  
567  
568  
569  
570  
571  
572  
573  
574  
575  
576  
577  
578  
579  
580  
581  
582  
583  
584  
585  
586



**A**

**MSK - IMPACT**



**B**

**KRAS Mutant**

Odds Ratio: 0.31  
P-value:  $1.44 \times 10^{-6}$

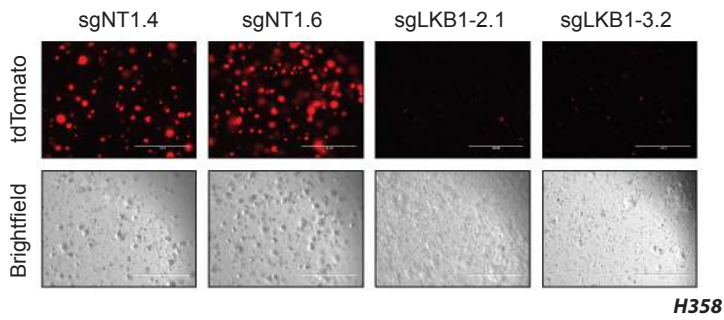
		TP53	
		WT	Mut
LKB1	WT	155	122
	Mut	103	25

**KRAS WT**

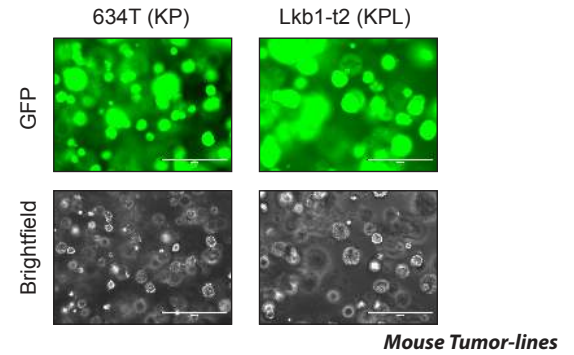
Odds Ratio: 1.13  
P-value: 0.56

		TP53	
		WT	Mut
LKB1	WT	348	481
	Mut	48	75

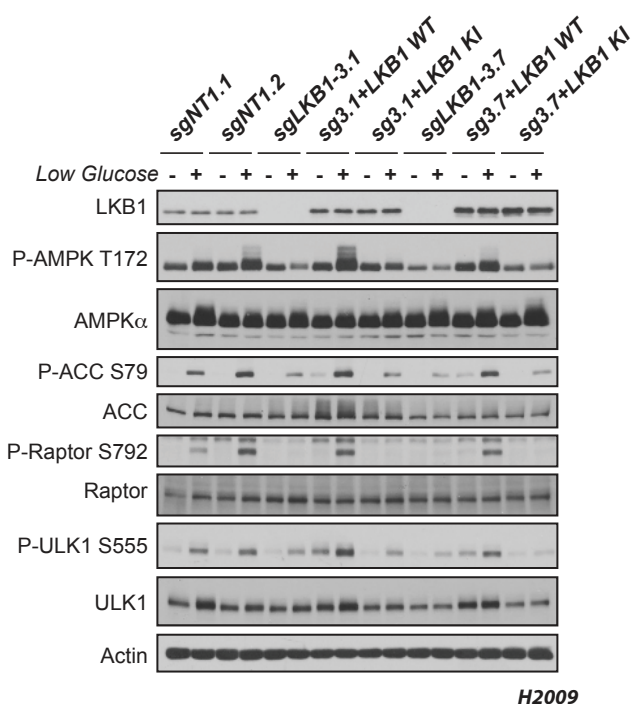
**C**



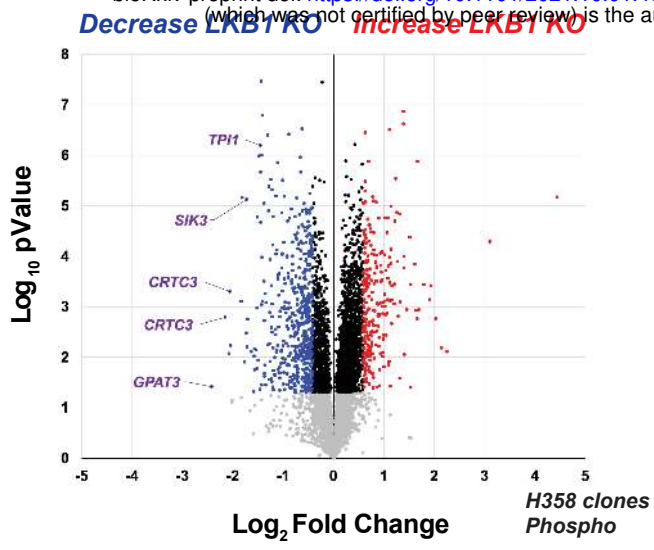
**D**



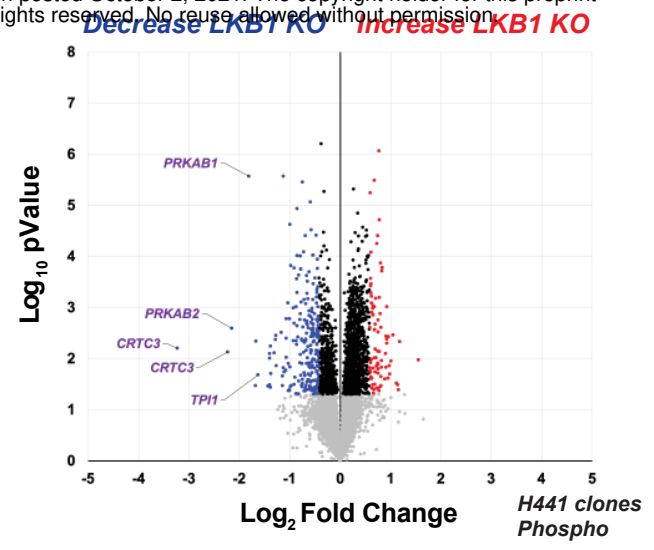
**E**



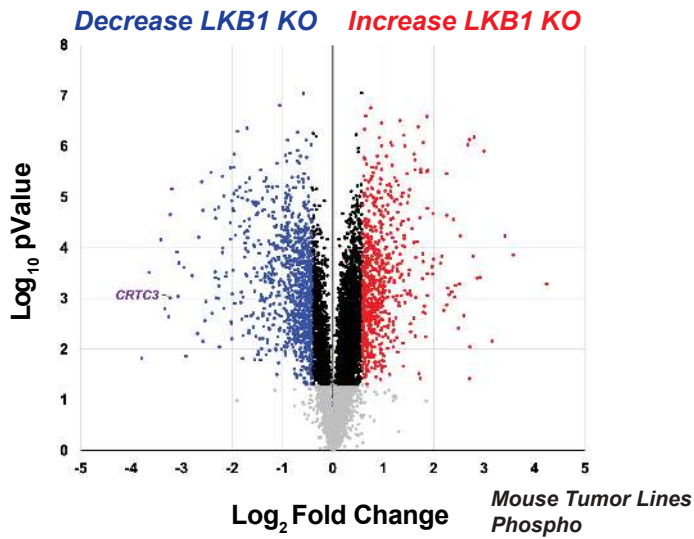
**A**



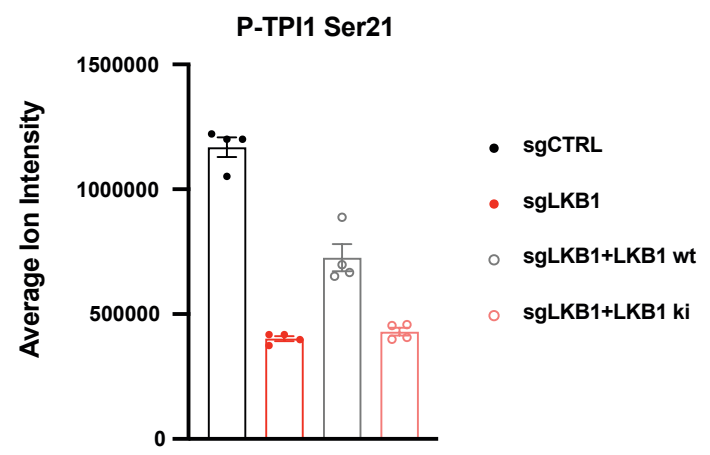
**B**



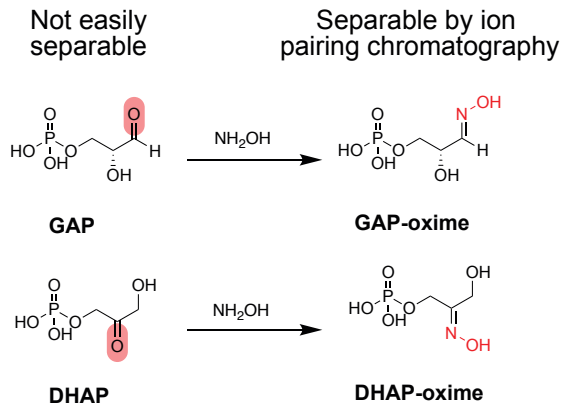
**C**



**D**



**E**



**F**

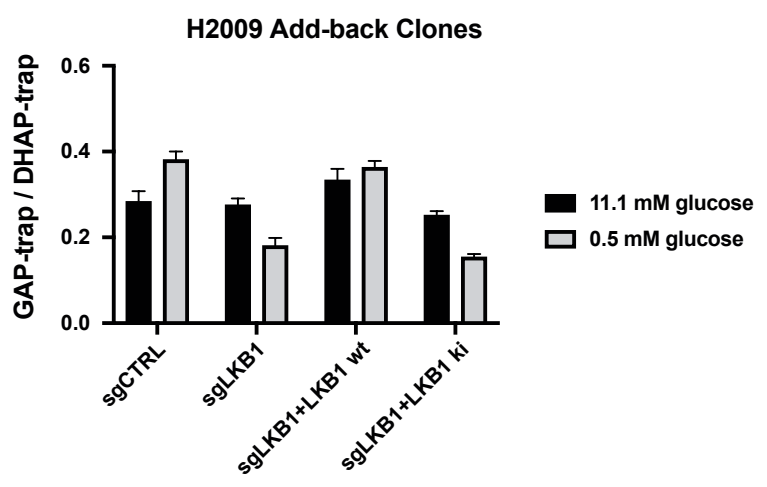
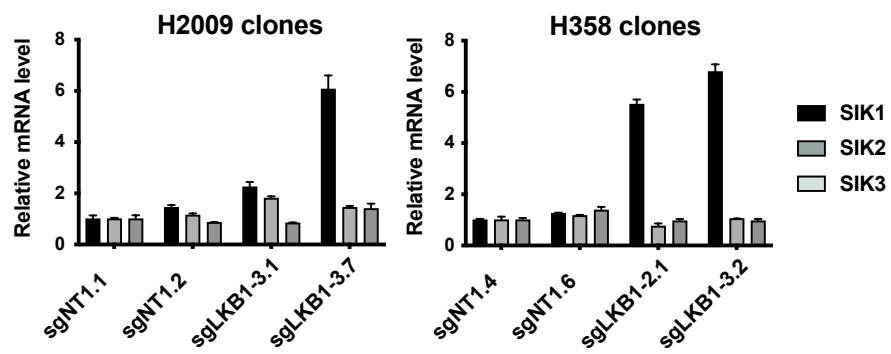
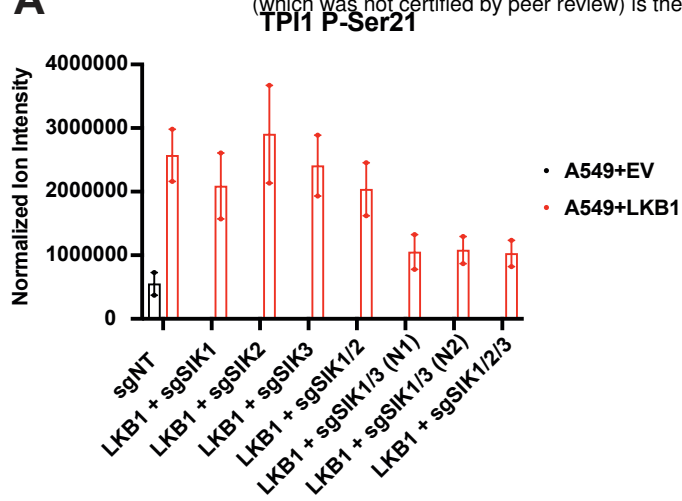
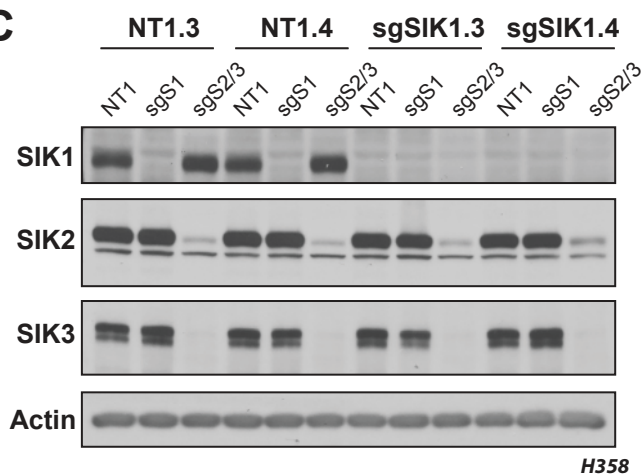


**Figure S2**

**A**



**C**



## 587 **Methods**

588

589 No statistical methods were used to predetermine sample size. Data were visualized and statistical  
590 analyses performed using Prism 9 software (Graph Pad) or R statistical package.  $P < 0.05$  was considered  
591 statistically significant.  $P$  values for paired comparisons between two groups with comparable variance were  
592 calculated by two-tailed Student's  $t$ -test.

593

## 594 **Reagents**

595 Media and sera were purchased from Life Technologies and R&D Systems respectively. All other reagents  
596 were from Sigma-Aldrich unless otherwise noted.

597

## 598 **Cell lines**

599 All cell lines (A549, H358, H441, H2009, 634T and HEK293T) were purchased from ATCC or kindly  
600 provided by Kwok-Kin Wong at NYU Langone Medical Center (634T and Lkb1-t2). Cells were maintained in  
601 RPMI 1640 medium (Life Technologies: 11879020) supplemented with glucose concentrations as indicated  
602 (Life Technologies: A2494001) except for HEK293T cells, which were propagated in DMEM with sodium  
603 pyruvate and L-glutamine (Corning). All media supplemented with 10% FBS, 100 units/ml of penicillin and  
604 100  $\mu\text{g/ml}$  streptomycin and grown at 37°C in a 5%  $\text{CO}_2$  humidified incubator. All cell lines were confirmed  
605 to be mycoplasma-free using the MycoAlert mycoplasma detection kit (Lonza: LT07-218).

606

## 607 **CRISPR/Cas9 reagents, plasmids**

608 The control and LKB1-KO lines were generated by infecting the cell lines with lentivirus generated from the  
609 LentiCRISPRv2 plasmid (Addgene: 52961). The control and TPI1-KO or SIK-KO lines were generated by  
610 infecting the Cas9-expressing lines (LentiCRISPRv2) with lentivirus generated from the LRT2B plasmid  
611 (Addgene: 110854). The sgRNA sequences are as follows: sgNT1, CCAATACGGACCGGATTGCT;  
612 sgLKB1-2, TGTATAACACATCCACCAGC; sgLKB1-3, TGCACAAGGACATCAAGCCG; sgSAFE,  
613 GGTGGATAAGGCTTAGAAA; sgTPI1-3, GAAGTACACGAGAAGCTCCG; sgTPI1-4,  
614 GGAAGCCATCCACATCAGGC; sgSIK1, ATGGTCGTGACAGTACTCCA; sgSIK2,  
615 GCACCGGATCACCAAGACGG; sgSIK3, GTGCTTGACAGATCTGCTCCA. The TPI1 alleles were  
616 synthesized by Twist Biosciences and cloned into pHAGE-CMV-N-Flag-HA-IRES-Puro-DEST via Gateway  
617 cloning.

618

## 619 **Lentivirus production, transduction and single-cell cloning**

620 Lentivirus was generated by transfecting the target plasmid with the packaging plasmids pMD2.G  
621 (Addgene: 12259) and psPAX2 (Addgene: 12260) into 293T cells using Lipofectamine 3000 (Invitrogen:  
622 L3000015). Media was changed 6 hours after transfection, and then the viral supernatant was collected at  
623 24 and 48h post-transfection. Transduction was conducted in 6 well format on  $1 \times 10^5$  cells and cells plated  
624 in suspension into viral supernatant containing 8  $\mu\text{g/ml}$  Polybrene (Santa Cruz Biotechnology: SC-134220)  
625 and incubated overnight (16h). Viral supernatant aspirated and fresh culturing media added to transduced  
626 cells for recovery for 24h. Puromycin (Life Technologies: A1113803) was supplemented into media 48h  
627 post-transduction for relevant plasmids (LentiCRISPRv2 and pHAGE-CMV-N-Flag-HA-IRES-PURO) at a  
628 concentration of 2  $\mu\text{g/ml}$  and selection conducted for 72h. Blasticidin (Invivogen: ANT-BL-1) was  
629 supplemented into media 48h post-transduction for relevant plasmid (LRT2B) at a concentration of 10  $\mu\text{g/ml}$   
630 and selection conducted for 5 days. Following selection, single cell cloning was conducted by serial dilution  
631 and plating into a 96 well plate, and cells were maintained under relevant selection criteria during the  
632 cloning process. Clones that grow out from single cells were expanded and validation of knockout  
633 conducted by western-blot or qPCR as indicated.

634

## 635 **LUAD clinical data set analysis.**

636 Human LUAD (hLUAD) datasets (TCGA and MSKCC) were downloaded from cBioPortal and KRAS, TP53,  
637 and LKB1 mutational and copy number status were assessed. Samples were divided into KRAS-mutant and  
638 KRAS-wild-type cohorts for further analysis. Using the R statistical software package, a Fisher's exact test  
639 was performed on each cohort to determine the odds of TP53 and LKB1 mutations co-occurring.

640

641 **Mice and xenografts.**

642 Animal procedures were performed with the approval of the Weill Cornell Medicine IACUC. Tumor volume  
643 was not allowed to exceed 1000 mm<sup>3</sup> in any experiment. Prior to implantation, cells were re-suspended in  
644 PBS and mixed 1:1 with Matrigel (Corning, 356231). Cells were then injected subcutaneously into single  
645 flanks of 6-week-old athymic mice (Envigo). Caliper measurements were performed weekly to monitor  
646 tumor growth. For the H358 LKB1-KO clones, 1 x 10<sup>6</sup> cells were injected per flank; for the murine lung  
647 tumor lines (634T and Lkb1-t2) 1 x 10<sup>4</sup> cells were injected per flank.

648  
649 **Western blotting**

650 Protein lysates were prepared in CST lysis buffer (Cell Signaling Technology: 9803) supplemented with  
651 cOmplete mini EDTA free protease inhibitor (Roche: 04693159001) and quantified using the BCA protein  
652 assay (Thermo Scientific, 23225). Lysates prepared at a concentration of 1 mg/ml and supplemented with  
653 4x Laemmli Sample Buffer (Bio-Rad: 1610747) supplemented with fresh 2-mercaptoethanol (Sigma:  
654 M3148). Proteins were separated on self-cast Tris-glycine polyacrylamide gels, transferred to Polyscreen  
655 PVDF membranes (Perkin Elmer: NEF1002), and probed with Cell Signaling Technology antibodies used at  
656 1:1000 in 5% BSA (Sigma: A4503) in TBS-T: P-ACC Ser79 (#3661), ACC (#3662), P-Raptor Ser792  
657 (#2083), Raptor (#2280), P-AMPK $\alpha$  Thr172 (#2535), AMPK  $\alpha$ 1/2 (#2532), LKB1 (#3047), P-ULK1 Ser555  
658 (#5869), ULK1 (#8054) and SIK2 (6919). Antibodies from Abcam used at concentrations indicated in 5%  
659 BSA in TBS-T against  $\beta$ -actin (ab6276, 1:20,000), TPI1 (ab96696, 1:3,000) and P-SIK1 Thr182 + P-SIK2  
660 Thr175 + P-SIK3 Thr163 (ab199474, 1:1000). Antibody from Novus Biologicals was used at 1:20,000 in 5%  
661 BSA in TBS-T against SIK3 (NBP2-47278). Antibodies from Sigma-Aldrich against Flag epitope tag  
662 (F7425, 1:5,000) and (F3165, 1:1000) were used at indicated concentrations in 5% BSA in TBS-T.  
663 Secondary antibodies from Millipore against Rabbit (AP132PMI) and Mouse (AP124PMI) primary antibodies  
664 were resuspended per manufacturer's instructions and used at 1:10,000 in 5% non-fat dried milk in TBS-T.  
665 Western blots were then developed in the dark room on an autoradiograph following incubation with home-  
666 made ECL.

667  
668 **Sn-glycerol-3-phosphate steady state analysis metabolite extraction**

669 Cells were cultured in medium reconstituted from glucose-free RPMI 1640 medium (Life Technologies:  
670 11879020) supplemented with 11.1 or 0.5 mM glucose and 10% dialyzed FBS. The day prior to treatment  
671 and collection cells were lifted and counted and 2 x 10<sup>6</sup> cells were plated in a 10cm culture dish. Cells were  
672 given a medium change 1 h before the addition of growth medium. Cells were rinsed twice with PBS before  
673 the addition of tracing medium. The time of addition of tracer medium was designated time 0. Metabolites  
674 were extracted at 30 minutes post addition as indicated in text.

675  
676 **Aqueous metabolite extraction and liquid chromatography–mass spectrometry (LC–MS) analysis**

677 Cells were washed twice with PBS, and twice with LC-MS grade H<sub>2</sub>O. Five hundred  $\mu$ l of 80% methanol at  
678  $-80^{\circ}\text{C}$  was added to quench metabolic reactions and the cells were collected by scraping. The lysate was  
679 then transferred to a fresh 2.0 ml Eppendorf tube pre-chilled on dry-ice and an additional 500  $\mu$ l of 80%  
680 methanol was added to the original plate and scraped again. The second lysate was added to the first and  
681 incubated on dry ice for 20 minutes with intermittent vortexing then centrifuged at 16,000g for 10 min to  
682 allow cellular debris to be pelleted. The aqueous volume was then transferred to a clean, fresh pre-chilled  
683 2.0 ml Eppendorf tube and dried under vacuum in a speedvac and stored at  $-80^{\circ}\text{C}$ . Dried sample pellets  
684 were resuspended in HPLC-grade water (20  $\mu$ l) and centrifuged at 20,000 g for 5 min to remove insoluble  
685 material. Following centrifugation, 16  $\mu$ l of supernatant was transferred to virgin polypropylene auto sampler  
686 vials, capped and placed on dry ice. Supernatants (5  $\mu$ l) were injected and analyzed using a hybrid 6500  
687 QTRAP triple quadrupole mass spectrometer (AB/SCIEX) coupled to a Prominence UFLC HPLC system  
688 (Shimadzu) via selected reaction monitoring (MRM). ESI voltage was +4900V in positive ion mode with a  
689 dwell time of 3 ms per SRM transition. Approximately 10–14 data points were acquired per detected  
690 metabolite. Samples were delivered to the mass spectrometer via hydrophilic interaction chromatography  
691 (HILIC) using a 4.6 mm i.d. x 10 cm Amide XBridge column (Waters) at 400  $\mu$ l/min. Gradients were run  
692 starting from 85% buffer B (HPLC grade acetonitrile) to 42% B from 0 to 5 min; 42% B to 0% B from 5 to 16  
693 min; 0% B was held from 16 to 24 min; 0% B to 85% B from 24 to 25 min; 85% B was held for 7 min to re-  
694 equilibrate the column. Buffer A was comprised of 20 mM ammonium hydroxide/20 mM ammonium acetate

695 (pH = 9.0) in 95:5 water:acetonitrile. Peak areas from the total ion current for each metabolite SRM  
696 transition were integrated using MultiQuant v3.0 software (AB/SCIEX). Tubes containing cellular debris was  
697 retained to determine protein concentration for data normalization. Briefly pellet was resuspended by  
698 addition of 600  $\mu$ l of sodium hydroxide and boiled at 90 °C for 30 minutes with intermittent vortexing.  
699 Resolubilized pellets were allowed to come to room temperature, and protein quantified using the DC  
700 protein assay (Bio-Rad: 5000111). Derived metabolite data was normalized to protein concentration and  
701 median ion intensity per injection across the dataset.  
702

### 703 ***In situ* hydroxylamine trapping in live cells**

704 Two 15 cm dishes per condition were plated with  $9 \times 10^6$  cells 24 hr prior to treatment. Plated cells were  
705 washed twice with PBS then grown in RPMI 1640 media containing 11.1 mM or 0.5 mM glucose as  
706 indicated for 6 hr. Cells were then washed twice with PBS and 3 ml of PBS containing protease inhibitors  
707 was added to the plate and cells were scraped. Cell homogenate was transferred to a 15ml conical tube  
708 and centrifuged at 1,400 x g for 3 minutes to pellet cells. Cellular pellets were resuspended in 300  $\mu$ l ice  
709 cold 80% Methanol and transferred to a 1.5 ml Eppendorf tube. Chemical labeling of live cells was  
710 achieved by adding 10  $\mu$ l of hydroxylamine solution (Sigma: 467804, ~15M solution) and incubated for 10  
711 minutes with gently vortexing intermittently. Following a 10 minute incubation, the suspended cells were  
712 lysed with a probe sonicator set to 30% amperage pulse (1:1 pulse:pause 16 seconds total). Lysed cellular  
713 homogenates were then centrifuged at 20,000 x g for 10 minutes at 4 °C. Clarified supernatant was  
714 transferred to a fresh 1.5 ml Eppendorf tube and dried under Nitrogen gas flow until all solvent was  
715 evaporated. Dried pellets were then stored at -80 °C until ready for analysis. Dried metabolites were  
716 resuspended in 100  $\mu$ L of an 80:20 mixture of MeOH/H<sub>2</sub>O and an internal deuterated standard, 10 nmol d<sub>3</sub>-  
717 serine, was added to the dried metabolome solution for quantification and sample normalization.  
718

### 719 **Targeted LC-MS/MS for hydroxylamine trapping**

720 Resuspended metabolites were separated by hydrophilic interaction chromatography with a Gemini  
721 reverse-phase C18 column (50 mm x 4.6 mm with 5  $\mu$ m diameter particles) from Phenomenex together with  
722 precolumn (C18, 3.5 mm, 2 mm X 20 mm). Mobile phase A was composed of 100% H<sub>2</sub>O (10 mM  
723 tributylamine aqueous solution, adjusted to pH 4.95 with 15 mM acetic acid), and mobile phase B was  
724 composed of 100% Methanol. Using a multi-step gradient with buffer A and B: 0-5 min, 95% A; 5-15 min,  
725 95-90% A; 15-22 min, 90-85% A; 22-26 min, 10% A, and maintained for 4 min; 30-33 min, 95% A, and  
726 maintained for 7 min. The flow rate was 0.2 ml/min for 0-15 min and 30-40 min, and 0.3 ml/min for 15-30  
727 min. Targeted MS/MS analysis was performed on an Agilent triple quadrupole LC-MS/MS instrument  
728 (Agilent Technologies 6460 QQQ). The capillary voltage was set to 4.0 kV. The drying gas temperature  
729 was 350°C, the drying gas flow rate was 10 L/min, and the nebulizer pressure was 45 psi. Relative  
730 metabolite abundance was quantified by integrated peak area for the given MRM-transition. Data  
731 presented are representative of three independent biological experiments each containing three technical  
732 replicates for a given condition.  
733

### 734 **Proteomics and phospho-proteomic sample preparation**

735 Protein lysates were prepared in CST lysis buffer (Cell Signaling Technology: 9803) supplemented with  
736 cComplete mini EDTA free protease inhibitor (Roche: 04693159001) and quantified using the BCA protein  
737 assay (Thermo Scientific, 23225). Following quantification, 100  $\mu$ g of each protein lysate was moved into a  
738 clean 1.5 mL tube. Following distribution of protein, each tube was brought to a final volume of 300  $\mu$ L by  
739 addition of PBS, followed by precipitation with trichloroacetic acid (TCA) (Sigma) to a final concentration of  
740 25%, vigorously vortexed and incubated on ice overnight. TCA precipitates were centrifuged at 21,130 x g  
741 for 30 minutes at 4°C, washed twice in 500  $\mu$ L of ice-cold acetone, and centrifuged at 21,130 x g for 10  
742 minutes after each wash. Following precipitation and washes, pellets were allowed to completely dry at  
743 room temperature. Dry pellets were re-suspended in 100  $\mu$ L of 100 mM TEAB, 0.5% SDS and reduced with  
744 9.5 mM tris-carboxyethyl phosphine (TCEP) for 60 minutes at 55°C. Following reduction of disulfide bonds  
745 with TCEP, the denatured protein mix was centrifuged at 21,130 x g for 5 minutes then alkylated with 4.5  
746 mM iodoacetamide (IA) for 30 minutes in the dark at room temperature. After reduction and alkylation of  
747 disulfide bonds, the denatured protein mixture was precipitated out of solution by addition of 600  $\mu$ L of ice-  
748 cold acetone and placed in the -20°C freezer overnight. The following day precipitated proteins were

749 centrifuged at 8,000 x g for 10 minutes to pellet precipitated protein. Following centrifugation supernatant  
750 was decanted off and pellets were allowed to air-dry at room temperature. Once dry, protein pellets were  
751 reconstituted in 100  $\mu$ L 100 mM TEAB and  $\text{CaCl}_2$  was supplemented to a final concentration of 1 mM, 2  $\mu$ g  
752 of sequencing grade Trypsin (Promega) was added, and reactions were placed in the dark on a thermal  
753 mixer (Eppendorf) set to 37°C and shaking at 850 r.p.m. for 16 hours.

### 754 **Thermal Proteomic Profiling**

755 Cells were lifted using TrypLE Express (Thermo Fisher Scientific - GIBCO) and neutralized following 5-  
756 minute incubation using complete media (RPMI + 10% FBS penicillin/streptomycin) and centrifuged at 1100  
757 r.p.m. for 4 minutes. The cell pellet was reconstituted in 10 mL PBS containing protease and phosphatase  
758 inhibitors (Roche) and centrifuged again at 1100 RPM for 4 minutes. Following centrifugation, the cell pellet  
759 was resuspended in 1 mL PBS with inhibitors and distributed into thin-wall PCR tubes at 100  $\mu$ L of cell  
760 suspension in each tube. Thermal denaturation was performed as previously described, and the resulting  
761 cellular suspension was transferred to clean 1.5 mL microcentrifuge tubes and PCR tubes were additionally  
762 rinsed with 30  $\mu$ L of PBS with inhibitors to ensure complete transfer of cellular suspension. Cellular  
763 suspension was next snap frozen in liquid nitrogen for 1 minute followed by thawing and re-equilibration  
764 back to room temperature. This freeze-thaw cycle was repeated 2 additional times and the soluble fraction  
765 of each lysate was generated by centrifugation at 21,130 x g for 30 minutes at 4°C. Supernatants were  
766 transferred to clean 1.5 mL microcentrifuge tubes, and protein was quantified in the supernatant for  
767 temperatures 37°C and 41°C by micro-BCA assay (Thermo Fisher Scientific - Pierce). Following  
768 quantification, the average of the two lowest temperatures was taken and the volume equivalent to 30  $\mu$ g of  
769 protein in the lowest temperature was moved from each temperature fraction into a clean 1.5 mL tube.  
770 Following distribution of protein, each tube was brought to a final volume of 300  $\mu$ L by addition of PBS with  
771 inhibitors, followed by precipitation with trichloroacetic acid (TCA) (Sigma) to a final concentration of 25%,  
772 vigorously vortexed and incubated on ice overnight. TCA precipitates were centrifuged at 21,130 x g for 30  
773 minutes at 4°C, washed twice in 500  $\mu$ L of ice-cold acetone, and centrifuged at 21,130 x g for 10 minutes  
774 after each wash. Following precipitation and washes, pellets were allowed to completely dry at room  
775 temperature. Dry pellets were re-suspended in 100  $\mu$ L of 100 mM TEAB, 0.5% SDS and reduced with 9.5  
776 mM tris-carboxyethyl phosphine (TCEP) for 60 minutes at 55°C. Following reduction of disulfide bonds with  
777 TCEP, the denatured protein mix was centrifuged at 21,130 x g for 5 minutes then alkylated with 4.5 mM  
778 iodoacetamide (IA) for 30 minutes in the dark at room temperature. After reduction and alkylation of  
779 disulfide bonds, the denatured protein mixture was precipitated out of solution by addition of 600  $\mu$ L of ice-  
780 cold acetone and placed in the -20°C freezer overnight. The following day precipitated proteins were  
781 centrifuged at 8,000 x g for 10 minutes to pellet precipitated protein. Following centrifugation supernatant  
782 was decanted off and pellets were allowed to air-dry at room temperature. Once dry, protein pellets were  
783 reconstituted in 100  $\mu$ L 100 mM TEAB and  $\text{CaCl}_2$  was supplemented to a final concentration of 1 mM, 1  $\mu$ g  
784 of sequencing grade Trypsin (Promega) was added, and reactions were placed in the dark on a thermal  
785 mixer (Eppendorf) set to 37°C and shaking at 850 r.p.m. for 16 hours. The next day, digested samples were  
786 centrifuged at 21,130 x g for 10 minutes and proceeded to TMT labeling of digested samples.

### 787 **TMT Labeling, Fractionation, and Phosphopeptide Enrichment**

788 TMT labeling was performed generally as per manufacturer's protocol. Briefly, each TMT tag was re-  
789 suspended in 164  $\mu$ L anhydrous acetonitrile with intermittent vortexing for 10 minutes. Following  
790 resuspension, 41  $\mu$ L was added to corresponding temperatures (TMT-126 = 37°C; four separate aliquots of  
791 each temperature for subsequent desalting and fractionation) and labeling reaction was allowed to proceed  
792 for 1 hour at room temperature. Reactions were quenched by addition of 8  $\mu$ L of 5% hydroxylamine in 100  
793 mM TEAB and incubated for 15 minutes. Labeled temperature fractions were pooled, desalted on 1cc/50  
794 mg C18 SepPAK columns (Waters # WAT054955) on a vacuum manifold and desalted peptides were dried  
795 down in a speedvac. Dried peptides were reconstituted in 300  $\mu$ L of 0.1% TFA in  $\text{H}_2\text{O}$ , high-pH reverse  
796 phase spin-columns (Thermo fisher scientific - Pierce) were equilibrated, and samples fractionated per  
797 manufacturer's instructions into 8 fractions, 2 washes and a flow-through fraction (11 total). Separate  
798 samples from the same fractions were then combined and dried. Peptide fractions were reconstituted in 200  
799  $\mu$ L of 5% acetonitrile, 0.1% TFA in water, and 10  $\mu$ L was removed for bulk HTP analysis. The remaining  
800 fractionated labeled peptides dried and re-dissolved in 40% acetonitrile, 6% TFA in water before  
801  
802

803 phosphopeptide enrichment with Titansphere 5  $\mu\text{m}$   $\text{TiO}_2$  beads (GL Sciences). Titansphere  $\text{TiO}_2$  beads (GL  
804 Sciences) were reconstituted in buffer containing 80% acetonitrile, 6% TFA, and 2,5-dihydroxybenzoic acid  
805 (20 mg/mL) and rotated for 15 min at 25°C. Equal amount of beads slurry (~5:1 beads-to-peptide ratio  
806 based on concentration of peptides in 37°C aliquot) was added to each temperature aliquot of reconstituted  
807 peptides and rotated for 20 mins 25°C. Beads were then washed twice with higher percentage of  
808 acetonitrile (10% and 40%) in 6% TFA and supernatant was removed by centrifugation at 500 x g for 2 min.  
809 Washed beads were then added to self-packed stage tip with C8 SPE (Sigma Aldrich) and washed once  
810 more with 60% acetonitrile in 6% TFA. Phosphopeptides were first eluted with 5%  $\text{NH}_4\text{OH}$ , then 10%  
811  $\text{NH}_4\text{OH}$ , 25% acetonitrile, and dried with speedvac. Dried phosphopeptides were reconstituted in 5%  
812 acetonitrile, 1% TFA, desalted with self-packed stage tip with C18 SPE (Sigma Aldrich), and dried with  
813 speedvac once more. The final processed phosphopeptides were reconstituted in 5% acetonitrile, 0.1%  
814 TFA in water for LC-MS<sup>3</sup> analysis.

815

### 816 **LC-MS<sup>3</sup> Analysis and Data Acquisition**

817 High-pH reverse-phase fractions were run on a 4-hour instrument method with an effective linear gradient of  
818 180 minutes from 5% to 25% mobile phase B with the following mobile phases: A: 0.1% formic acid in  $\text{H}_2\text{O}$ ,  
819 B: 80% acetonitrile/0.1% formic acid in water on a 50 cm Acclaim PepMap RSLC C18 column (Thermo  
820 Fisher Scientific #164942) operated by a Dionex ultimate 3000 RSLC nano pump with column heating at  
821 50°C connected to an Orbitrap Fusion Lumos. Briefly, the instrument method was a data-dependent  
822 analysis and cycle time set to 3 seconds, total. Each cycle consisted of one full-scan mass spectrum (400-  
823 1500  $m/z$ ) at a resolution of 120,000, RF Lens: 60%, maximum injection time of 100 ms followed by data-  
824 dependent MS/MS spectra with precursor selection determined by the following parameters: AGC Target of  
825  $4.0e^5$ , maximum injection time of 100 ms, monoisotopic peak determination: peptide, charge state inclusion:  
826 2-7, dynamic exclusion 10 sec with an intensity threshold filter:  $5.0e^3$ . Data-dependent MS/MS spectra were  
827 generated by isolating in the quadrupole with an isolation window of 0.4  $m/z$  with CID activation and  
828 corresponding collision energy of 35%, CID activation time of 10 ms, activation Q of 0.25, detector type Ion  
829 Trap in Turbo mode, AGC target of  $1.0e4$  and maximum injection time of 120 ms. Data-dependent multi-  
830 notch MS<sup>3</sup> was done in synchronous precursor selection mode (SPS, multi-notch MS<sup>3</sup>) with the following  
831 settings: Precursor selection Range; Mass Range 400-1200, Precursor Ion Exclusion Properties  $m/z$  Low:  
832 18 High: 5, Isobaric Tag Loss Exclusion Properties: TMT. Number of SPS precursors was set to 10 and  
833 data-dependent MS<sup>3</sup> was detected in the Orbitrap (60,000 resolution, scan range 120-500) with an isolation  
834 window of 2  $m/z$  HCD activation type with collision energy of 55%, AGC target of  $1.2e5$  and a maximum  
835 injection time of 150 ms. Raw files were parsed into MS1, MS2 and MS3 spectra using RawConverter.

836

### 837 **Proteomic, phospho-proteomic and Thermal Profiling Data Analysis**

838 Data generated were searched using the ProLuCID algorithm in the Integrated Proteomics Pipeline (IP2)  
839 software platform. Human and Mouse proteome data were searched using concatenated target/decoy  
840 UniProt databases. Basic searches were performed with the following search parameters: HCD  
841 fragmentation method; monoisotopic precursor ions; high resolution mode (3 isotopic peaks); precursor  
842 mass range 600-6,000 and initial fragment tolerance at 600 p.p.m.; enzyme cleavage specificity at C-  
843 terminal lysine and arginine residues with 3 missed cleavage sites permitted; static modification of  
844 +57.02146 on cysteine (carboxyamidomethylation), +229.1629 on N-terminal and lysine for TMT-10-plex  
845 tag; 4 total differential modification sites per peptide, including oxidized methionine (+15.9949), and  
846 phosphorylation (+79.9663) on serine, threonine, and tyrosine (only for phospho-enriched samples); primary  
847 scoring type by XCorr and secondary by Zscore; minimum peptide length of six residues with a candidate  
848 peptide threshold of 500. A minimum of one peptide per protein and half-tryptic peptide specificity were  
849 required. Starting statistics were performed with a  $\Delta\text{mass}$  cutoff = 10 p.p.m. with modstat, and trypstat  
850 settings. False-discovery rates of protein (pfp) were set to 1% (for unenriched datasets) or peptide (sfp) set  
851 to 1% (for phospho-proteomics datasets). TMT quantification was performed using the isobaric labeling 10-  
852 plex labeling algorithm, with a mass tolerance of 5.0 p.p.m. or less. Reporter ions 126.127726, 127.124761,  
853 127.131081, 128.128116, 128.134436, 129.131417, 129.13779, 130.134825, 130.141145, and 131.13838  
854 were used for relative quantification.

855



856 **References:**

- 857 1 Siegel, R. L., Miller, K. D. & Jemal, A. Cancer statistics, 2020. *CA Cancer J Clin* **70**, 7-30,  
858 doi:10.3322/caac.21590 (2020).
- 859 2 Pavlova, N. N. & Thompson, C. B. The Emerging Hallmarks of Cancer Metabolism. *Cell Metab* **23**,  
860 27-47, doi:10.1016/j.cmet.2015.12.006 (2016).
- 861 3 Chen, P. H. *et al.* Metabolic Diversity in Human Non-Small Cell Lung Cancer Cells. *Mol Cell* **76**, 838-  
862 851 e835, doi:10.1016/j.molcel.2019.08.028 (2019).
- 863 4 Demetrius, L. Of mice and men. When it comes to studying ageing and the means to slow it down,  
864 mice are not just small humans. *EMBO Rep* **6 Spec No**, S39-44, doi:10.1038/sj.embor.7400422  
865 (2005).
- 866 5 Zehir, A. *et al.* Mutational landscape of metastatic cancer revealed from prospective clinical  
867 sequencing of 10,000 patients. *Nat Med* **23**, 703-713, doi:10.1038/nm.4333 (2017).
- 868 6 Eichner, L. J. *et al.* Genetic Analysis Reveals AMPK Is Required to Support Tumor Growth in Murine  
869 Kras-Dependent Lung Cancer Models. *Cell Metab* **29**, 285-302 e287, doi:10.1016/j.cmet.2018.10.005  
870 (2019).
- 871 7 Hollstein, P. E. *et al.* The AMPK-Related Kinases SIK1 and SIK3 Mediate Key Tumor-Suppressive  
872 Effects of LKB1 in NSCLC. *Cancer Discov* **9**, 1606-1627, doi:10.1158/2159-8290.CD-18-1261 (2019).
- 873 8 Liu, Y. *et al.* Metabolic and functional genomic studies identify deoxythymidylate kinase as a target in  
874 LKB1-mutant lung cancer. *Cancer Discov* **3**, 870-879, doi:10.1158/2159-8290.CD-13-0015 (2013).
- 875 9 Rogers, Z. N. *et al.* Mapping the in vivo fitness landscape of lung adenocarcinoma tumor suppression  
876 in mice. *Nature Genetics* **50**, 483-486, doi:10.1038/s41588-018-0083-2 (2018).
- 877 10 Orozco, J. M. *et al.* Dihydroxyacetone phosphate signals glucose availability to mTORC1. *Nature*  
878 *Metabolism* **2**, 893-901, doi:10.1038/s42255-020-0250-5 (2020).
- 879 11 Anastasiou, D. *et al.* Inhibition of Pyruvate Kinase M2 by Reactive Oxygen Species Contributes to  
880 Cellular Antioxidant Responses. *Science* **334**, 1278-1283, doi:10.1126/science.1211485 (2011).
- 881 12 Cheung, E. C. *et al.* Dynamic ROS Control by TIGAR Regulates the Initiation and Progression of  
882 Pancreatic Cancer. *Cancer Cell* **37**, 168-182.e164, doi:10.1016/j.ccell.2019.12.012 (2020).
- 883 13 DeNicola, G. M. *et al.* Oncogene-induced Nrf2 transcription promotes ROS detoxification and  
884 tumorigenesis. *Nature* **475**, 106-109, doi:10.1038/nature10189 (2011).
- 885 14 Chang, J. W., Lee, G., Coukos, J. S. & Moellering, R. E. Profiling Reactive Metabolites via Chemical  
886 Trapping and Targeted Mass Spectrometry. *Analytical Chemistry* **88**, 6658-6661,  
887 doi:10.1021/acs.analchem.6b02009 (2016).
- 888 15 Roland, B. P. *et al.* Triosephosphate isomerase I170V alters catalytic site, enhances stability and  
889 induces pathology in a Drosophila model of TPI deficiency. *Biochim Biophys Acta* **1852**, 61-69,  
890 doi:10.1016/j.bbadis.2014.10.010 (2015).
- 891 16 Savitski, M. M. *et al.* Tracking cancer drugs in living cells by thermal profiling of the proteome. *Science*  
892 **346**, 1255784, doi:10.1126/science.1255784 (2014).
- 893 17 Huang, J. X. *et al.* High throughput discovery of functional protein modifications by Hotspot Thermal  
894 Profiling. *Nature Methods* **16**, 894-901, doi:10.1038/s41592-019-0499-3 (2019).
- 895 18 Faubert, B. *et al.* Loss of the tumor suppressor LKB1 promotes metabolic reprogramming of cancer  
896 cells via HIF-1 $\alpha$ . *Proceedings of the National Academy of Sciences* **111**, 2554-2559,  
897 doi:10.1073/pnas.1312570111 (2014).
- 898 19 Xu, H. G. *et al.* LKB1 reduces ROS-mediated cell damage via activation of p38. *Oncogene* **34**, 3848-  
899 3859, doi:10.1038/onc.2014.315 (2015).
- 900 20 Li, F. *et al.* LKB1 Inactivation Elicits a Redox Imbalance to Modulate Non-small Cell Lung Cancer  
901 Plasticity and Therapeutic Response. *Cancer Cell* **27**, 698-711,  
902 doi:https://doi.org/10.1016/j.ccell.2015.04.001 (2015).
- 903 21 Kim, J. *et al.* CPS1 maintains pyrimidine pools and DNA synthesis in KRAS/LKB1-mutant lung cancer  
904 cells. *Nature* **546**, 168-172, doi:10.1038/nature22359 (2017).
- 905 22 Shackelford, D. B. & Shaw, R. J. The LKB1-AMPK pathway: metabolism and growth control in tumour  
906 suppression. *Nature Reviews Cancer* **9**, 563-575, doi:10.1038/nrc2676 (2009).
- 907 23 Sun, Z., Jiang, Q., Li, J. & Guo, J. The potent roles of salt-inducible kinases (SIKs) in metabolic  
908 homeostasis and tumorigenesis. *Signal Transduction and Targeted Therapy* **5**, 150,  
909 doi:10.1038/s41392-020-00265-w (2020).

- 910 24 Sakamoto, K., Bultot, L. & Göransson, O. The Salt-Inducible Kinases: Emerging Metabolic Regulators.  
911 *Trends in Endocrinology & Metabolism* **29**, 827-840, doi:10.1016/j.tem.2018.09.007 (2018).
- 912 25 Berggreen, C., Henriksson, E., Jones, H. A., Morrice, N. & Göransson, O. cAMP-elevation mediated  
913 by  $\beta$ -adrenergic stimulation inhibits salt-inducible kinase (SIK) 3 activity in adipocytes. *Cellular*  
914 *Signalling* **24**, 1863-1871, doi:<https://doi.org/10.1016/j.cellsig.2012.05.001> (2012).
- 915 26 Itoh, Y. *et al.* Salt-inducible Kinase 3 Signaling Is Important for the Gluconeogenic Programs in Mouse  
916 Hepatocytes \*. *Journal of Biological Chemistry* **290**, 17879-17893, doi:10.1074/jbc.M115.640821  
917 (2015).
- 918 27 DuPage, M., Mazumdar, C., Schmidt, L. M., Cheung, A. F. & Jacks, T. Expression of tumour-specific  
919 antigens underlies cancer immunoediting. *Nature* **482**, 405-409, doi:10.1038/nature10803 (2012).
- 920 28 Ngo, B. *et al.* Limited Environmental Serine and Glycine Confer Brain Metastasis Sensitivity to PHGDH  
921 Inhibition. *Cancer Discovery* **10**, 1352-1373, doi:10.1158/2159-8290.Cd-19-1228 (2020).
- 922 29 Murray, C. W. *et al.* An LKB1-SIK Axis Suppresses Lung Tumor Growth and Controls Differentiation.  
923 *Cancer Discov* **9**, 1590-1605, doi:10.1158/2159-8290.CD-18-1237 (2019).
- 924 30 Garcia, D. & Shaw, R. J. AMPK: Mechanisms of Cellular Energy Sensing and Restoration of Metabolic  
925 Balance. *Molecular Cell* **66**, 789-800, doi:10.1016/j.molcel.2017.05.032 (2017).
- 926